Pergamon

PII: S0042-6989(97)00086-2

Vision Res., Vol. 37, No. 20, pp. 2849–2869, 1997

Printed in Great Britain
0042-6989/97 $17.00 + 0.00

Similar Mechanisms Underlie Simultaneous Brightness Contrast and Grating Induction

BARBARA BLAKESLEE,*† MARK E. McCOURT*

Received 15 October 1996; in revised form 18 March 1997

The experiments explore whether the mechanism(s) underlying grating induction (GI) can also account for simultaneous brightness contrast (SBC). At each of three test field heights (1, 3 and 6 deg), point-by-point brightness matches were obtained from two subjects for test field widths of 32 deg (GI condition), 14, 12, 8, 6, 3 and 1 deg. The point-by-point brightness matches were quantitatively compared, using GI condition matches as a standard, to assess systematic alterations in the structure and average magnitude of brightness and darkness induction within the test fields as a function of changing test field height and width. In the wider test fields induction structure was present and was generally well-accounted for by the GI condition sinewave predictions. As test field width decreased the sinewave amplitude of the induced structure in the test field decreased (i.e., flattened), and eventually became negative (i.e., showed a reverse cusping) at the narrower test field widths. As expected, both subjects showed a decrease in overall levels of brightness and darkness induction with increasing test field height. For any particular test field height, however, relative brightness increased with decreasing test field width. This brightness increase began at larger test field widths as test field height increased. The results are parsimoniously accounted for by the output of a weighted, octave-interval array of seven difference-of-gaussian filters. This array of filters differs from those previously employed to model various aspects of spatial vision in that it includes filters tuned to much lower spatial frequencies. The two-dimensional output of this same array of filters also accounts for the GI demonstrations of Zaidi [(1989) *Vision Research, 29,* 691–697], Shapley and Reid's [(1985) *Proceedings of the National Academy of Sciences USA, 82,* 5983–5986] contrast and assimilation demonstration, and the induced spots seen at the street intersections of the Hermann Grid. The physiological plausibility of the filter array explanation of brightness induction is discussed, along with a consideration of its relationship to other models of brightness perception. © 1997 Elsevier Science Ltd

Brightness Induction Simultaneous brightness contrast Classical brightness contrast
Grating induction Filling-in

INTRODUCTION

It has long been known that the brightness of a region of visual space is not related solely to that region's luminance, but depends also upon the luminances of adjacent regions. Simultaneous brightness contrast (SBC) produces a homogeneous brightness change within an enclosed test field, such that a gray patch on a white background looks darker than an equiluminant gray patch on a black background. This effect has been well-quantified with respect to inducing background and test field luminance (Heinemann, 1955). Although SBC decreases with increasing test field size, brightness induction occurs for test fields as large as 10 deg (Yund & Armington, 1975). Since this distance far exceeds the dimensions of retinal or LGN receptive fields in monkey (DeValois & Pease, 1971; Yund *et al.*, 1977; DeValois & DeValois, 1988), a common explanation for SBC is that the brightness of the test field must be determined by the information at the edges of the bounded region (for example, by average perimeter contrast) and is subsequently filled-in or assigned to the entire enclosed area (Shapley & Enroth-Cugell, 1984; Cornsweet & Teller, 1965; Grossberg & Todorovic, 1988; Paradiso & Nakayama, 1991; Rossi & Paradiso, 1996; Paradiso & Hahn, 1996; for review see Kingdom & Moulden, 1988). It is becoming clear, however, that this explanation is too simple and that distal factors must also play a role in SBC (Arend *et al.*, 1971; Land & McCann, 1971; Heinemann, 1972; Shapley & Reid, 1985; Reid & Shapley, 1988).

Grating induction (GI) is a brightness effect that produces a spatial brightness variation (a grating) in an extended test field (McCourt, 1982). The perceived contrast of the induced grating decreases with increasing inducing grating frequency and with increasing test field

*Department of Psychology, North Dakota State University, Fargo, ND 58105-5075, U.S.A.
†To whom all correspondence should be addressed [*Fax*: +1-701-231-8426; *Email*: blakesle@prairie.nodak.edu].

height (McCourt, 1982), such that canceling contrast is constant for a constant product of inducing frequency and test field height (McCourt, 1982; Foley & McCourt, 1985). Although not formally reported for test fields larger than 3 deg, where at low frequencies the percentage of inducing grating contrast required to cancel the induced grating may still exceed 30% (McCourt, 1982), GI is observed in test fields at least as large as 6 deg (see Fig. 4). Although GI may extend over large distances, *homogeneous* brightness fill-in cannot account for GI. For example, a fill-in mechanism dependent on average perimeter contrast does not predict the appearance of a pattern in a GI test field because only a single value (average perimeter contrast) determines the assignment of brightness. A homogeneous fill-in mechanism which computes brightness based on local contrast rather than on average perimeter contrast (and which can therefore produce both positive and negative brightness signals originating from the opposite-polarity test field edges) still cannot produce a patterned test field (i.e., an induced grating). This is so because, without boundaries within the test field to arrest the propagation of these putative brightness signals, induced brightness and darkness will diffuse and average to produce the percept of a homogeneous test field. Several more complex brightness models have been proposed that incorporate non-homogeneous fill-in mechanisms (Grossberg & Mingolla, 1987; Pessoa *et al.*, 1995), but these have not yet been applied to GI.

It has been suggested that GI might be understood in terms of the output of parallel spatial filtering across multiple spatial scales (Moulden & Kingdom, 1991). An attractive feature of this approach is that both the low-pass spatial frequency response of GI, and the invariance of induction magnitude with viewing distance (i.e., the direct tradeoff between the effects of inducing grating spatial frequency and test field height), can be parsimoniously accounted for by multiple-channel isotropic spatial filtering.

Despite the fact that SBC is typically considered a homogeneous brightness effect dependent on homogeneous brightness fill-in, whereas the defining characteristic of grating induction is that it possesses spatial structure and cannot be produced by a homogeneous fill-in mechanism, it has nevertheless been suggested both that SBC is a special low frequency instance of grating induction (McCourt, 1982), and that GI is a particular case of SBC (Zaidi, 1989; Moulden & Kingdom, 1991). The present experiment explores this issue, asking whether the mechanism(s) underlying GI can account for SBC as well, or if fundamentally different brightness mechanisms are required to explain these effects. The structure and magnitude of induction in both GI and SBC stimuli were measured, where the inducing conditions for the two effects were rendered as similar as possible by employing one cycle of a low frequency sinewave grating as the inducer. Test field dimensions spanned a range that incorporated both classic SBC and GI configurations. Point-by-point brightness matches were quantitatively compared, using GI matches as a standard, to assess systematic changes in induction structure and magnitude as a function of changing test field height and width. Predictions from homogeneous brightness fill-in mechanisms as opposed to linear filtering mechanisms were compared. The results are most simply accounted for by the output of a weighted octave-interval array of difference-of-gaussian (DOG) filters. This array of filters differs from those previously employed to model various aspects of spatial vision in that it includes filters tuned to much lower spatial frequencies.

METHODS

Subjects

Two subjects (the authors BB and MM) participated in the study. Both subjects were well-practiced psychophysical observers and possessed normal or corrected-to-normal vision.

Instrumentation

Stimuli were generated using a PC-compatible microcomputer (486/66 MHz) with a custom-modified TIGA (Texas Instruments Graphics Architecture) graphics controller (Vision Research Graphics, Inc.). Images were presented on a high-resolution display monitor (21" IDEK Iiyama Vision Master, model MF-8221). Display format was 1024 (w) × 768 (h) pixels. Frame refresh rate was 97 Hz (non-interlaced). All images could possess 2^8 simultaneously presentable linearized intensity levels selected from a palette of approximately 2^{15}.

Stimuli

Viewed from a distance of 60.7 cm the stimulus field subtended 24.2 deg in height and 32 deg in width; individual pixels measured 0.031 deg × 0.031 deg. Mean display luminance was 50 cd/m^2. Inducing patterns appeared in the lower half of the stimulus field. The inducing patterns for all stimuli consisted of one cycle of a vertical sinewave grating (presented in sine phase) with a spatial frequency of 0.03125 cycles/degree (c/d). Inducing grating Michelson contrast was constant at 0.75. The test and comparison patches of classical SBC are both referred to here as test fields. The test fields were centered vertically within the inducing field and horizontally with respect to the half cycle of the sinewave in which they were inserted, e.g., Fig. 1(g). The luminance of the test fields was set to the mean luminance of the display (50 cd/m^2). GI test fields [see Fig. 1(a)] were unitary and extended the full width of the display (32 deg).

The height of the SBC and GI test fields assumed three values (1, 3 and 6 deg). Although increases in test field height resulted in decreases in inducing field height, the height of the upper and lower inducing fields was never less than 3 deg. Foley & McCourt (1985) demonstrated that GI magnitude remains constant until the sizes of the upper and lower inducing fields fall below this value. Therefore, the decreases in inducing field height

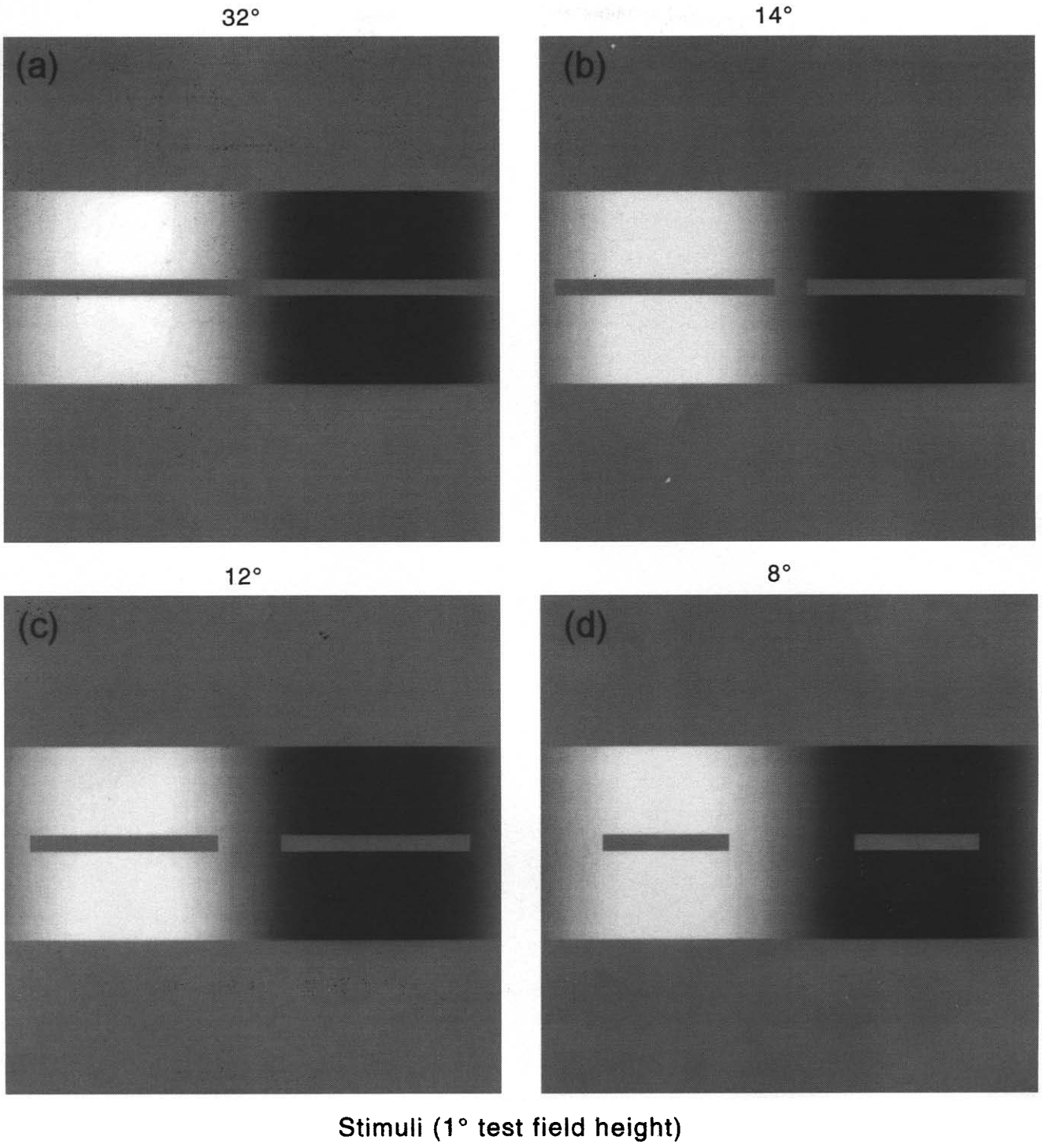

FIGURE 1(a–d). *Caption overleaf.*

produced by increasing test field height are not expected to alter GI magnitude. At each test field height the following test field widths were examined: 1, 3, 6, 8, 12, 14 and 32 deg. See Fig. 1(a–g) for illustrations of the stimuli used in the 1 deg test field height condition. The upper half of the stimulus display contained a matching stimulus of adjustable luminance surrounded by a homogeneous field which was also set to the mean luminance of the display (50 cd/m^2). The matching stimulus measured 0.25 deg in width and either 1, 3 or 6 deg in height, such that it was always matched in height to the test field under study.

Procedures

All stimuli were viewed binocularly through natural pupils in a dimly lit room. Each subject's head was positioned relative to the display with a chin and forehead rest. Eye movements were restricted only in that subjects were instructed to maintain their gaze within the display in order to hold adaptation state stable. Induction

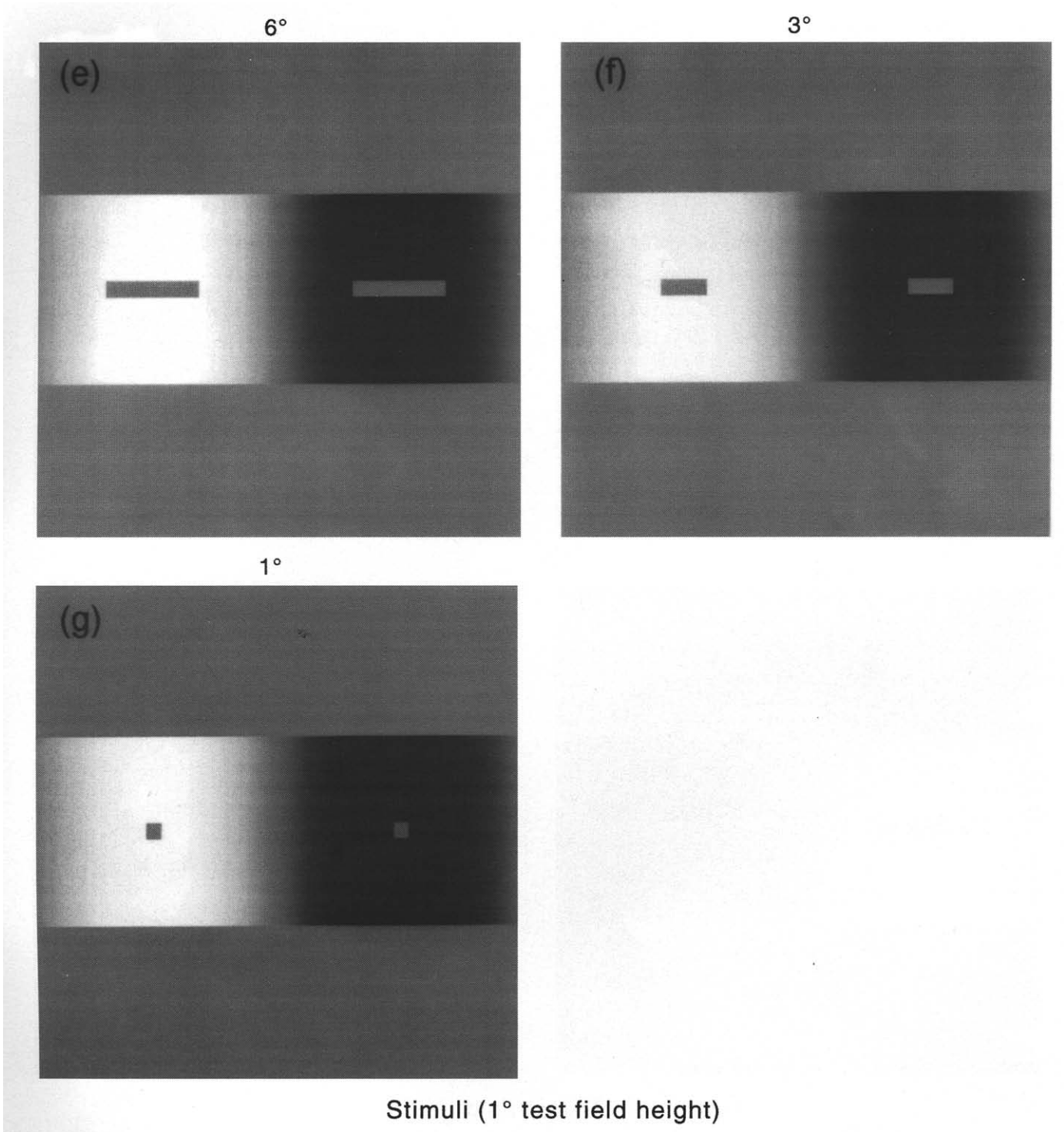

FIGURE 1. Stimuli used to measure the effect of test field width on induction magnitude. Test field widths of 32, 14, 12, 8, 6, 3 and 1 deg were tested at each of three test field heights (1, 3 and 6 deg). Only the stimuli from the 1 deg test field height condition are illustrated. Inducing contrast was constant at 0.75. Test field luminance was set to the mean of the display (50 cd/m^2). Note that the 32 deg stimulus is a standard GI stimulus (one unitary test field), the 1 deg stimulus is a "classical" SBC stimulus (two 1 deg×1 deg test fields). In the 3 and 6 deg test field height conditions the "classical" SBC stimulus is represented by the 3 and 6 deg test field width conditions, respectively.

magnitude was measured using a point-by-point brightness matching technique (Heinemann, 1972; McCourt, 1994). A thin bright line (1 pixel wide, 0.031 deg) served as a pointer. Subjects adjusted the luminance of the matching field (located several degrees directly above the pointer), until it matched the brightness of that region of the display (test field or inducing grating) to which the pointer referred. This region was located several degrees below the pointer (at the level of the test fields). Each trial was initiated by the subject. The initial luminance of the

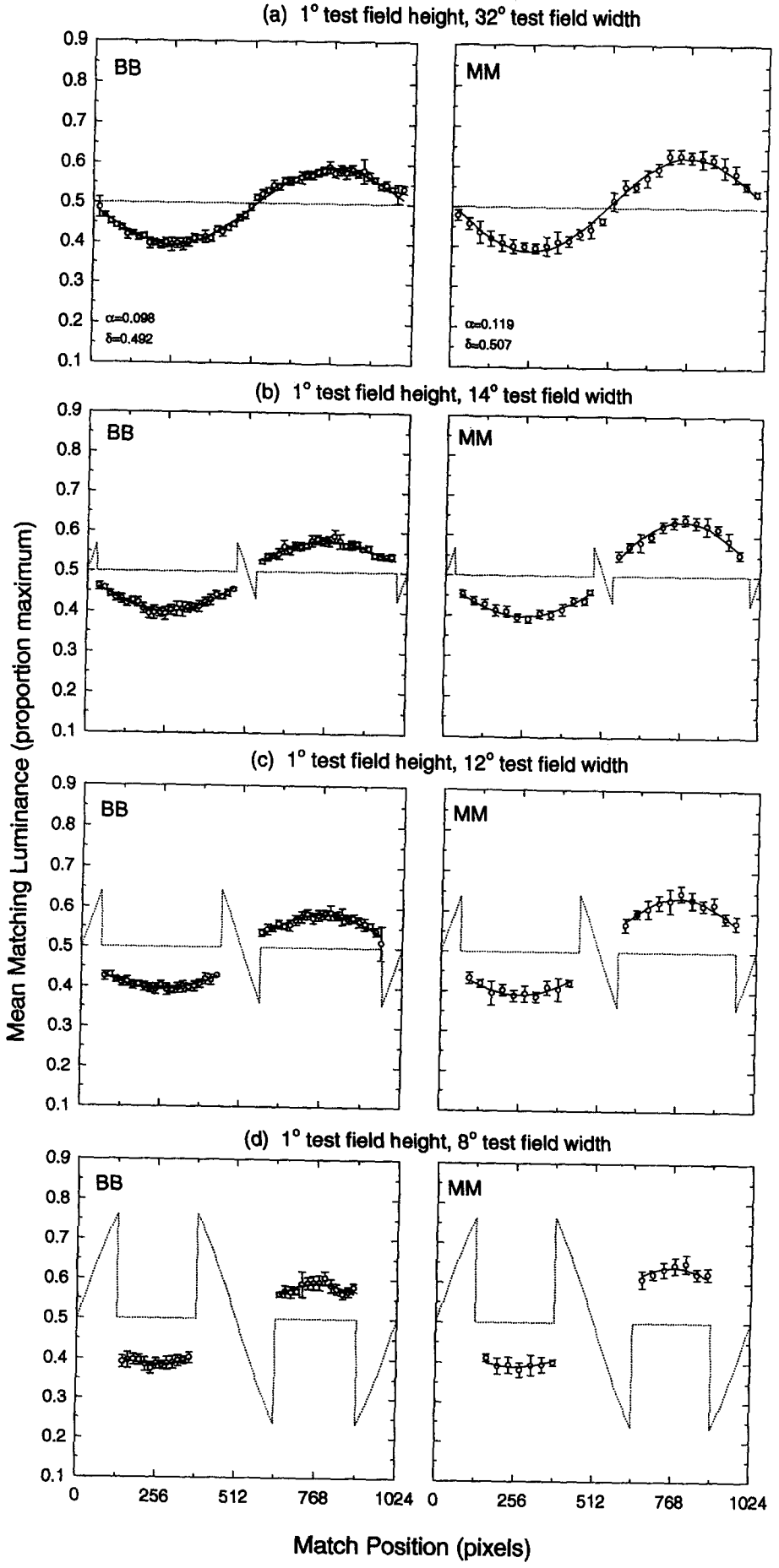

FIGURE 2 (a–d). *Caption overleaf.*

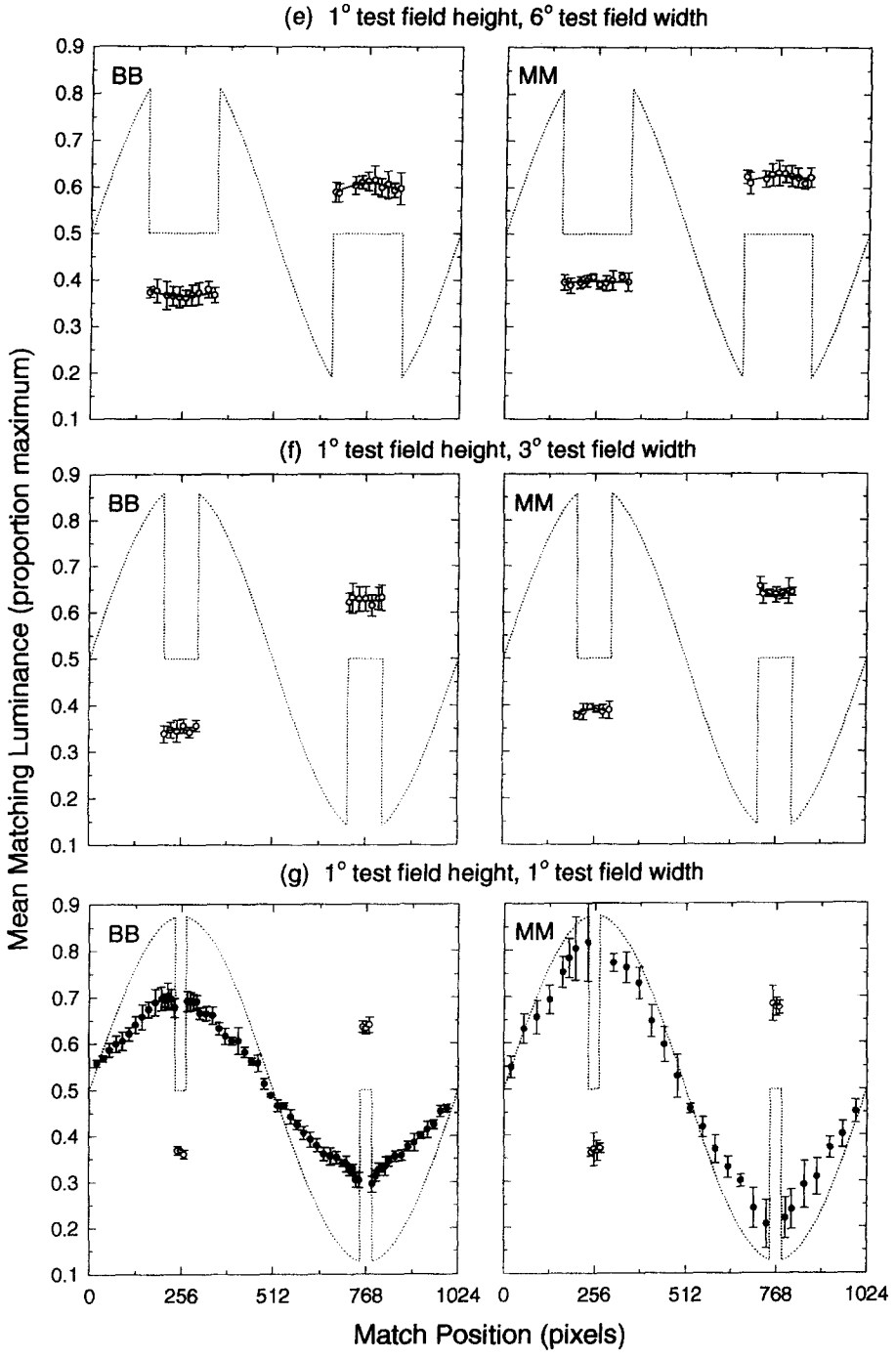

FIGURE 2. Complete sets of point-by-point brightness matches for subjects BB and MM are illustrated for the 1 deg test field height condition. Open symbols refer to brightness matches made to the test field(s); filled symbols are brightness matches to the inducing grating. The dotted line depicts the veridical luminance profile of the stimulus display along the vertical center of the test field. Mean luminance matches for each observer in the GI condition (32 deg test field width) were fit using a nonlinear regression procedure (method of least-squares) to a sinewave grating [Eq. (1)]. This optimized function is depicted by the solid line. The amplitude and offset parameters obtained from the 32 deg test field condition (GI) are referred to as the "grating induction prediction" and were used as a baseline to compare induction structure and magnitude for the narrower test field widths. These values are indicated in the panel for the 32 deg test field condition. Mean luminance matches in the 14, 12, 8, 6 and 3 deg test field conditions were modeled using a four-parameter version of Eq. (1). Eq. (2) permits independent amplitude variations within the dark and bright test fields. Parameters α_d and α_b refer to the amplitudes of the best-fitting sinewave functions to the mean luminance match values in the dark and bright half-cycles, respectively. Parameters δ_d and δ_b permit compensatory offset changes which accommodate magnitude changes produced by variations in parameters α_d and α_b. The best-fitting functions (solid lines) obtained for each stimulus configuration are indicated in each panel.

matching field was randomized at the beginning of each adjustment trial and subjects controlled subsequent increments and decrements in matching luminance by depressing appropriate response buttons. Each button press resulted in a matching field luminance change of 1 cd/m^2 (1.0% maximum luminance). No time limits

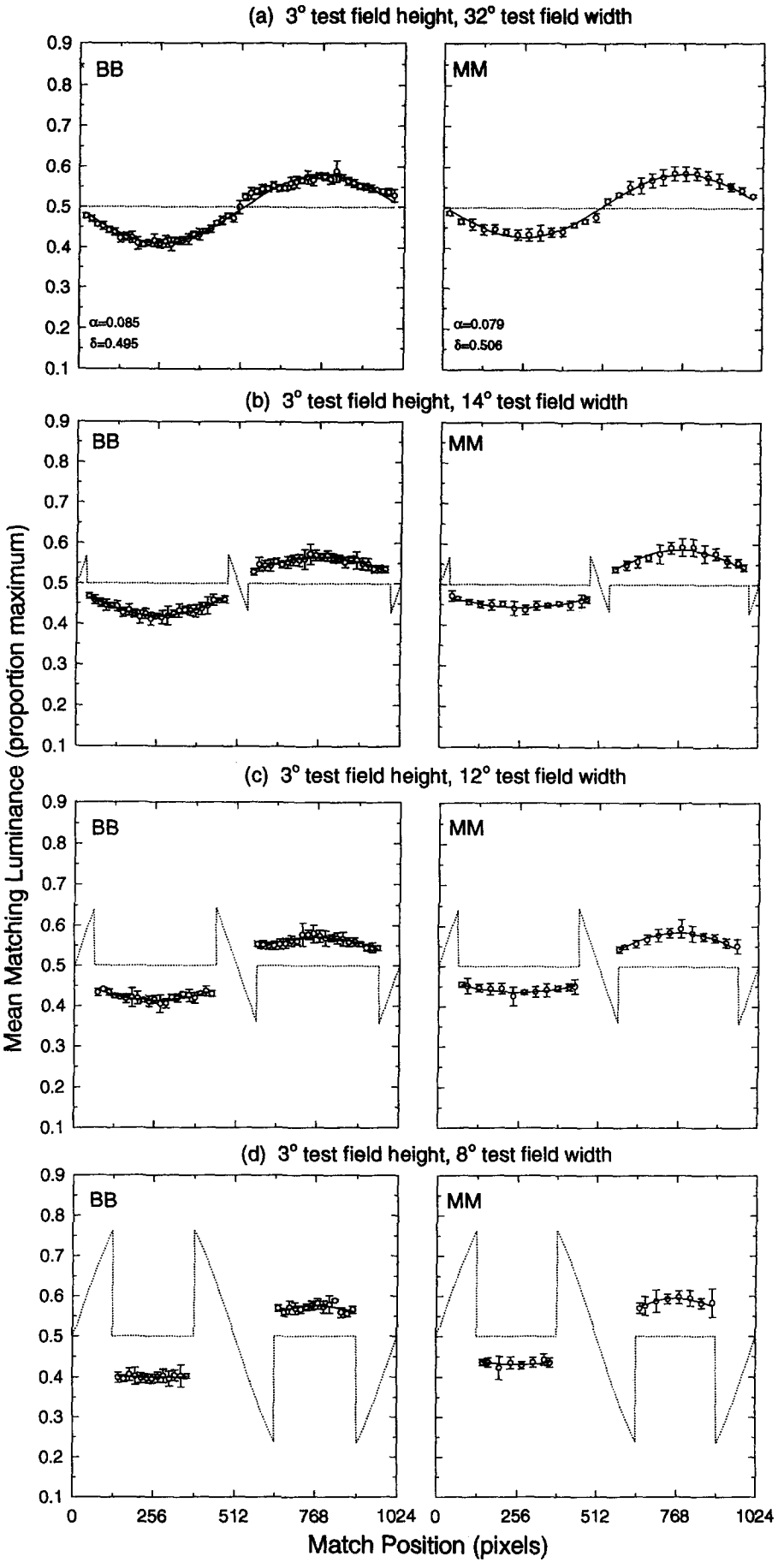

FIGURE 3 (a–d). *Caption overleaf.*

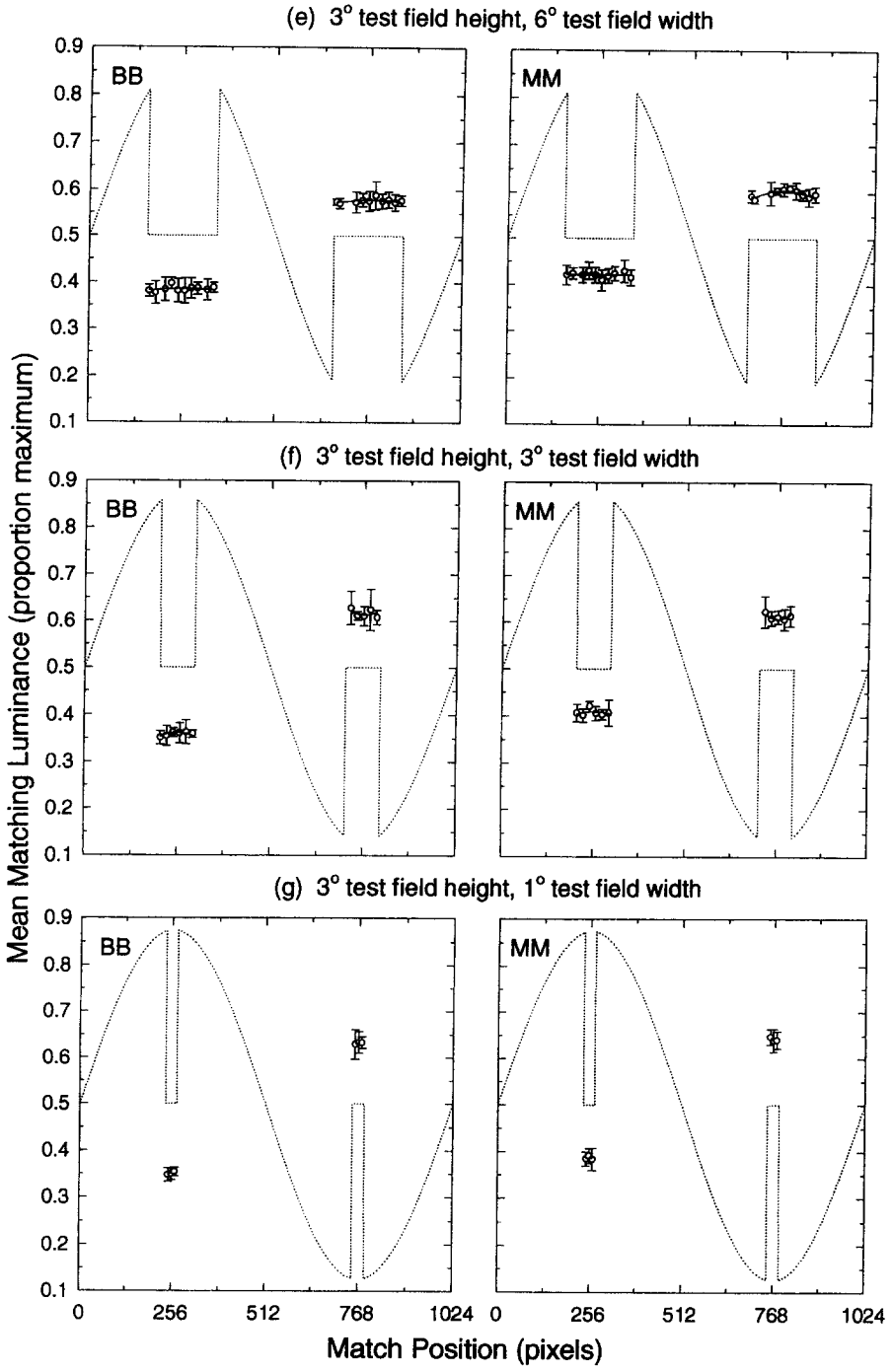

FIGURE 3. Complete set of point-by-point brightness matches for subjects BB and MM for the 3 deg test field height condition. See Fig. 2 for details.

were imposed, and the adjustment interval for each trial lasted until terminated by the subject. Final adjustment settings were recorded by computer, which also randomized the location of the matching field from trial to trial. Between five and ten matches were obtained from each subject in each experimental condition.

Under the conditions of the present experiment the percepts of brightness and lightness are not separable (Arend & Spehar, 1993a,b) and the term brightness is employed throughout when discussing the experimental results.

RESULTS

Mean matching luminance was compared across all stimuli. Complete sets of point-by-point brightness matches for the 1, 3 and 6 deg test field height conditions are illustrated for observers MM and BB in Figs 2–4. Open symbols refer to brightness matches made to the test field(s); filled symbols [Fig. 2(g)] are brightness matches to the inducing grating. The dotted line in each panel depicts the veridical luminance profile of the stimulus display along the vertical center of the test field.

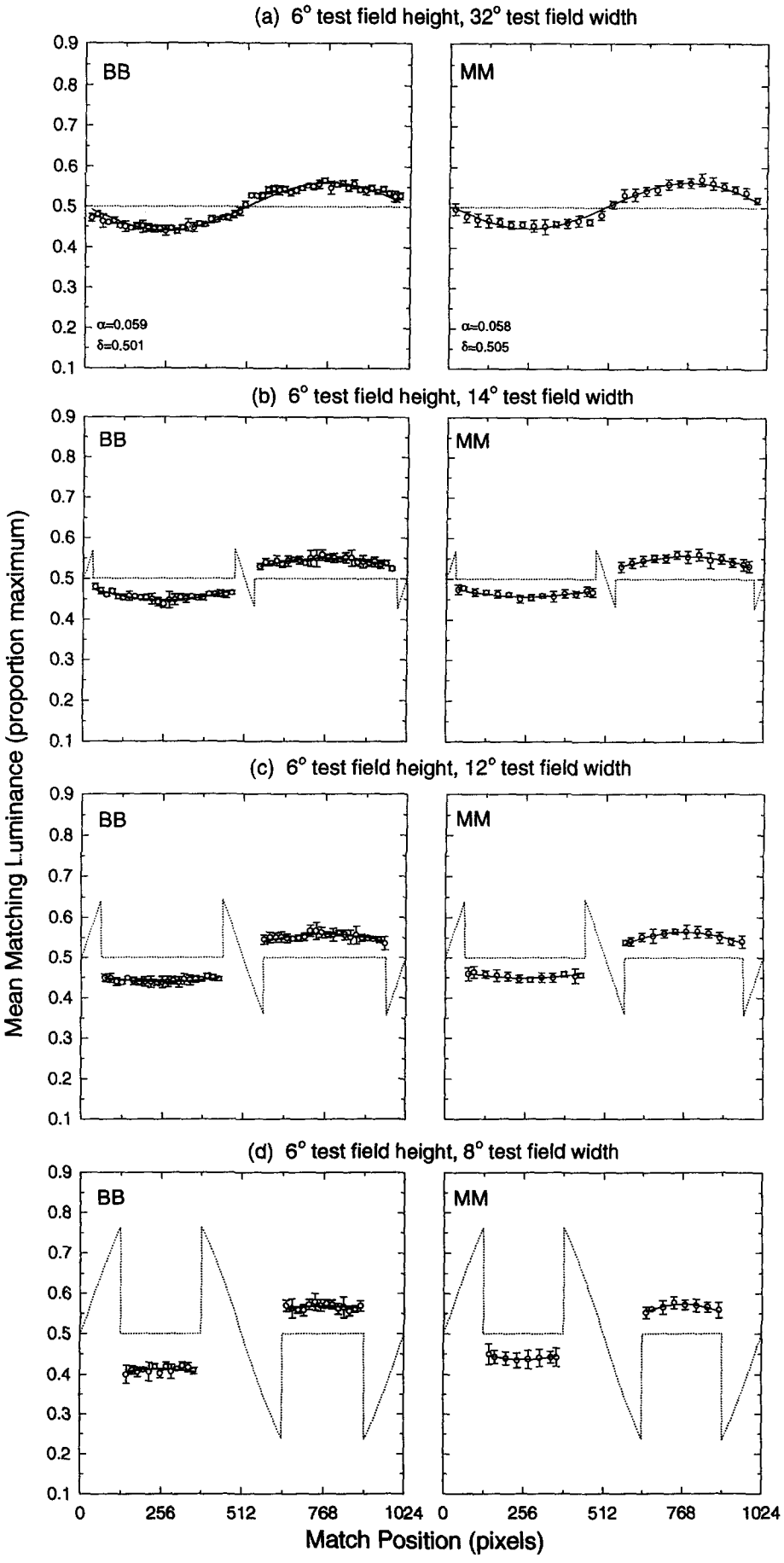

FIGURE 4 (a–d). *Caption overleaf.*

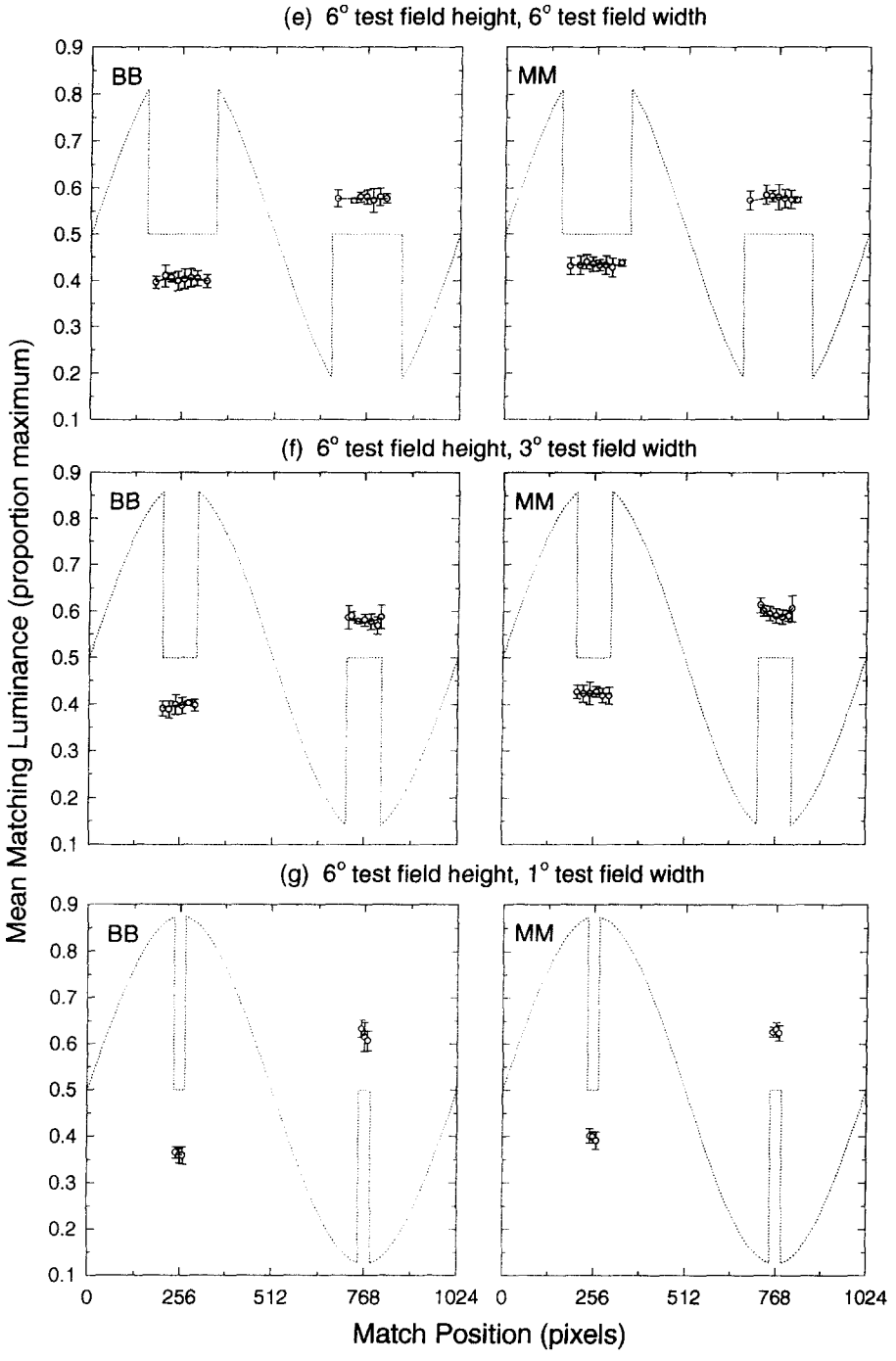

FIGURE 4. Complete set of point-by-point brightness matches for subjects BB and MM for the 6 deg test field height condition. See Fig. 2 for details.

Note that although the magnitude of GI decreases with increasing test field height (McCourt, 1982; Foley & McCourt, 1985), it is still clearly evident even in the 6 deg test field height condition. Similarly, brightness induction in SBC stimuli also decreases with increasing test field height and width (Yund & Armington, 1975). It is also of interest that both subjects show consistent undermatching to the inducing grating [see Fig. 2(g)].

Mean matching luminance values obtained from the point-by-point brightness matching procedure were analyzed to extract and quantify two key items of information: (1) Are changes in test field height and width accompanied by systematic alterations in the *structure* of the brightness variations within the test fields?; and (2) Do these changes cause systematic alterations in the *average magnitude* of brightness or darkness induction within the test fields?

The mean luminance matches of each observer in the GI condition (32 deg test field width) were fit using a nonlinear regression procedure (method of least-squares) to a sinusoidal function of the form:

$$L_M(\alpha, \delta, x) = -\alpha[\sin(x) + \delta] \qquad (1)$$

where the parameters α and δ refer to the amplitude and

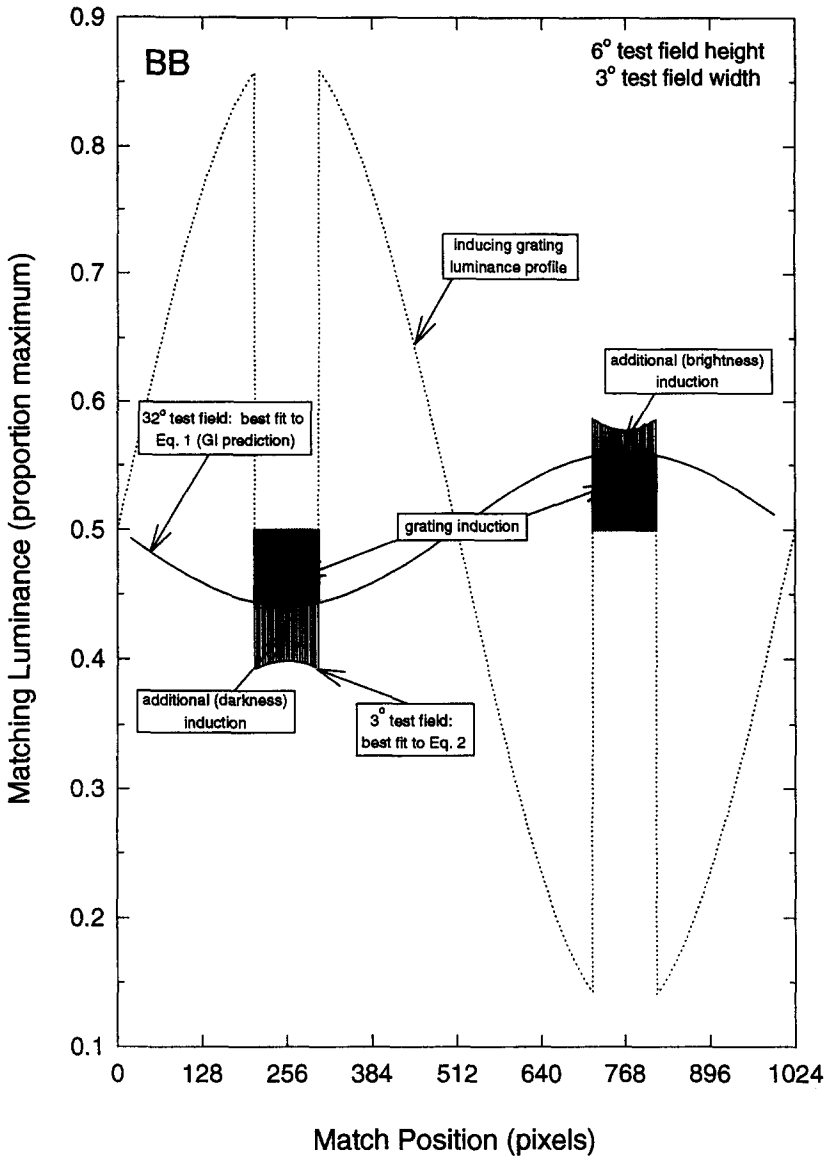

FIGURE 5. Illustration of the data analysis used to extract changes in the magnitude of induction which might accompany variations in test field width. The area between the veridical luminance distribution and the grating induction prediction [Eq. (1)] was numerically integrated for each observer. This area is illustrated by the bold hatched region. For each test field width the area between the grating induction prediction and the fit to the four-parameter function for that test field width [Eq. (2)] was also numerically integrated. The ratio of these two areas provides a comprehensive index of the average change in induction magnitude as a function of changing test field width.

offset of the matching function, respectively, and x refers to the spatial position of the brightness match. This optimized function is depicted by the solid line in Fig. 5 which illustrates the analysis, and by the solid lines in Figs 2(a), 3(a) and 4(a). The optimal parameter values obtained from the 32 deg test field (GI) condition are referred to as the "grating induction prediction". These parameter values are indicated in the legends of Figs 2(a), 3(a) and 4(a), and were used as a baseline to compare induction structure and magnitude in conditions where test field width was varied. To quantify changes in the *structure* of induction that occur with decreasing test field width, mean luminance matches in the 14, 12, 8, 6 and 3 deg test field conditions were modeled using a four-parameter version of Eq. (1):

$$L_M(\alpha_d, \alpha_b, \delta_d, \delta_b, x) = -\alpha_d[\sin(x) + \delta_d], x \leq \pi \text{ radians}$$
$$-\alpha_b[\sin(x) + \delta_b], x > \pi \text{ radians} \quad (2)$$

Eq. (2) permits independent amplitude variations within the dark and bright test fields. Parameters α_d and α_b refer to the amplitudes of the best-fitting sinewave functions to the mean luminance match values in the dark and bright half-cycles, respectively. Parameter x refers to the spatial position of the brightness match. Parameters δ_d and δ_b permit compensatory offset changes which accommodate magnitude changes produced by variations in parameters α_d and α_b. The best-fitting functions (solid lines) obtained for each stimulus configuration are

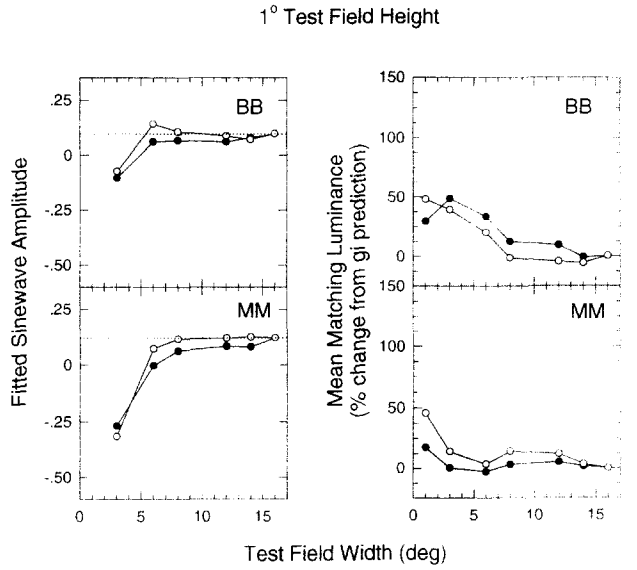

FIGURE 6. Summary of the matching data for subjects BB and MM obtained for the 1 deg test field height conditions using the best-fitting amplitude parameter and the index of induction magnitude. The left panels plot fitted sinewave amplitudes as a function of test field width for brightness induction (open symbols) and darkness induction (filled symbols). The dotted line represents the amplitude of the GI prediction. A decrease in the amplitude of the sinewave from the GI prediction indicates a flattening of the structure of the induction. Negative amplitudes indicate a reverse cusping in the structure of the induction relative to the GI prediction. The right panels summarize the matching data with respect to induction magnitude by plotting mean matching luminance (the % change from the GI prediction) as a function of test field width.

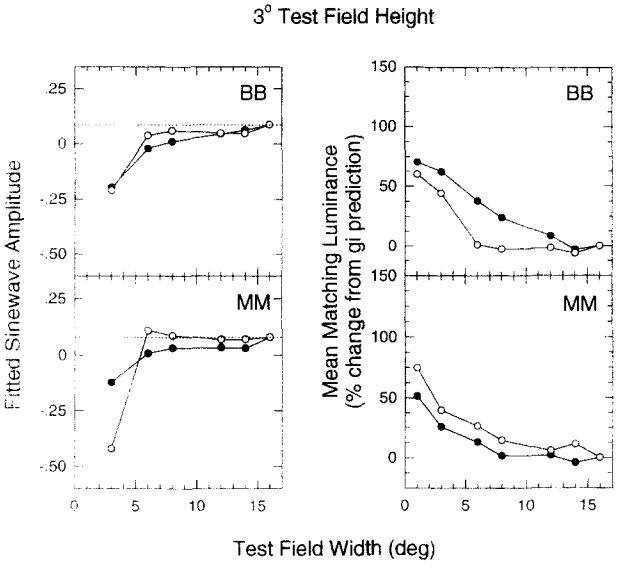

FIGURE 7. Summary of the matching data obtained for the 3 deg test field height. See Fig. 6 for details.

indicated in Figs 2(b–g), 3(b–g) and 4(b–g). Note that if the brightness variation within a test field is unchanged from the grating induction prediction, then the values of parameters α_d and α_b will equal α. If the brightness variations are "flattened" (i.e., are more squarewave than sinewave), however, then the values of α_d and α_b will approach zero. Finally, if the brightness variations within the test fields are opposite in spatial phase to those observed in the 32 deg wide grating induction test fields (i.e., if a reverse phase "cusping" occurs, such as in a missing-fundamental squarewave stimulus), such "cusping" will be indexed by negative values of parameters α_d and α_b.

Figures 6(left), 7(left) and 8(left) summarize the amplitude data. The structure of both brightness and darkness induction is generally well-accounted for by the GI predictions (horizontal dotted line) for test field widths of 14, 12 and 8 deg at all three test field heights. For test fields narrower than 8 deg in width, however, the tendency was for the amplitude parameters (α_d and α_b) to decrease and eventually assume negative values. This appears in the matching data as a flattening of the sinewave structure in the test fields [see Figs 2(e), 3(e) and 4(e)] followed by a reverse cusping [see Figs 2(f), 3(f) and 4(f)]. The 1 deg test field width condition was excluded from the amplitude analysis because the number of brightness matches (sampling rate) within this test field size was insufficient to assess structure in any meaningful way.

In order to index changes in the *magnitude* of induction which might accompany variations in test field width, the area between veridical matching (i.e., mean luminance) and the grating induction prediction [Eq. (1)] was numerically integrated for each observer at each test field height. This area is illustrated by the bold hatched region in Fig. 5. For each test field width the area between the grating induction prediction and the optimal fit to the four-parameter function for that test field width [Eq. (2)] was also numerically integrated. The ratio of these two areas provides a comprehensive index of the average change in induction magnitude as a function of changing

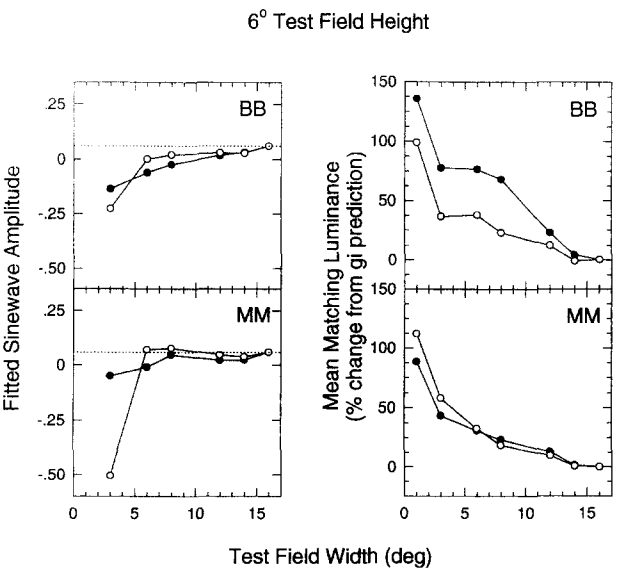

FIGURE 8. Summary of the matching data obtained for the 6 deg test field height. See Fig. 6 for details.

test field width. Although excluded from the amplitude analysis, the 1 deg test field condition was included in the induction magnitude analysis by setting the values of parameters α_d and α_b equal to 0 (i.e., by assuming a flat brightness profile across the test field). Hence, for this condition the values of parameters δ_d and δ_b alone index induction magnitude.

With respect to induction magnitude, Figs 6(right), 7(right) and 8(right) reveal that both subjects displayed a relative increase in both brightness and darkness induction with decreasing test field width. There was, in addition, a tendency for this relative increase in induction magnitude to be greater, and to begin at increasingly larger test field widths as test field height increased. Note that GI magnitude decreases with increasing test field height and that the increases in induction magnitude with decreasing test field width are relative to the GI prediction for that particular test field height. It is interesting that whereas for one subject the relative magnitude of brightness induction exceeded that of darkness induction, the opposite pattern was obtained for the second subject. This asymmetry is also obvious in the point-by-point brightness matching data of these subjects [see Figs 2–4]. These differences suggest that the relative gain of the "on" and "off" pathways in individual observers may differ in subtle, but perhaps meaningful ways. Further consideration of these intriguing differences is, however, beyond the scope of the present paper.

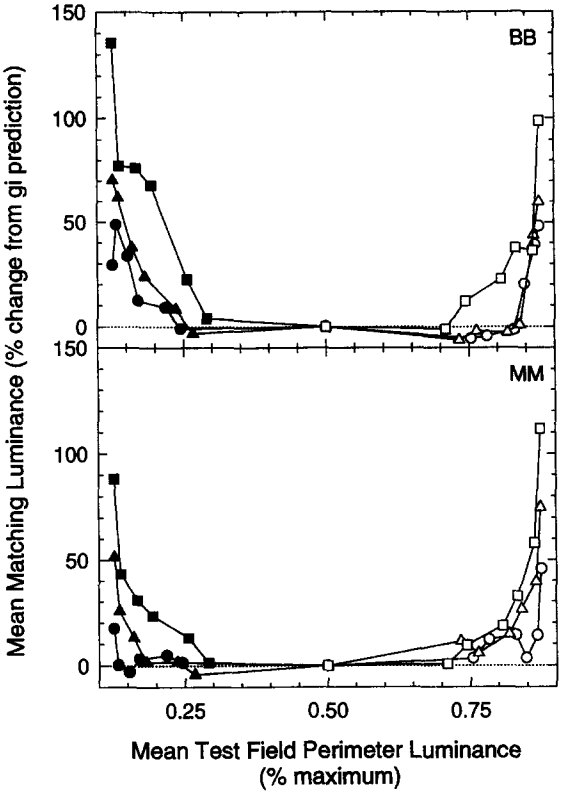

FIGURE 9. Mean matching luminance (the % change from the GI prediction) is plotted as a function of mean test field perimeter luminance for subjects BB and MM at three test field heights: 1 deg (circles), 3 deg (triangles) and 6 deg (squares). It is clear for both darkness (filled symbols) and brightness (open symbols) induction that a large change in mean test field perimeter luminance occurs before there is any corresponding shift in mean matching luminance from the GI prediction. Note that the curves representing the three test field height conditions are not congruent.

DISCUSSION

The mechanisms of induction

As discussed earlier, a *homogeneous* fill-in mechanism does not predict GI. In addition, the point-by-point matching data from the present study reveal no discontinuities in either the *structure* or *magnitude* of induction as the test field is transformed from the GI configuration (32 deg continuous test field) in which the mean perimeter luminance is equal to the mean, to the elongated but separate test fields (14 and 12 deg) in which mean perimeter luminance is substantially different for the two test fields situated on the bright and dark phases of the inducing grating. Clearly, a homogeneous fill-in mechanism cannot predict either the observed induction structure or the lack of a change in induction magnitude from the GI prediction in the elongated, but separate, test fields [see Figs 2(b, c), 3(b, c) and 4(b, c)]. These data are consistent, however, with the hypothesis that a single mechanism (which is not a homogeneous fill-in mechanism) underlies brightness induction in these elongated test field stimuli.

Consider next the change from the GI prediction in both structure (flattening) and magnitude (increase) that occurs with further decreases in test field width. Figure 9 indexes induction magnitude by plotting mean matching luminance (as a percent change from the GI prediction) as a function of mean test field perimeter luminance. It is clear for both darkness (filled symbols) and brightness (open symbols) induction that a large change in mean test field perimeter luminance occurs before there is any corresponding shift in mean matching luminance from the GI prediction. If a fill-in mechanism dependent on mean perimeter luminance is responsible for these systematic changes in induction magnitude as test field width decreases, it would have to possess a high contrast threshold (and/or a strongly accelerating continuous response nonlinearity), since a substantial change ($\pm 25\%$) in mean perimeter luminance is required before induction magnitude departs significantly from the GI prediction. This is inconsistent with results which indicate that the border contrast-dependent fill-in mechanism responsible for the missing-fundamental illusion possesses a low contrast threshold (Burr, 1987), and that induced brightness in the missing-fundamental square-wave illusion increases only for border contrasts up to 0.02, and actually declines with increasing contrast. A further difficulty for a fill-in explanation based solely on mean perimeter luminance is that the curves representing the three test field height conditions are not congruent (Fig. 9). Thus, to account for the differences in perceived brightness which are associated with regions possessing identical mean perimeter luminance, the putative homogeneous fill-in mechanism must assign brightness based

not only on mean perimeter luminance, but also on the geometry of the enclosed region. Even if such a homogeneous high-threshold fill-in mechanism could explain the increased magnitude of induction and the decreased amplitude (i.e., the "flattening") of induction structure at intermediate test field widths, it still cannot account for the reverse phase "cusping" observed at the narrower test field widths. Indeed, such "cusping" has almost universally been attributed to an edge or border contrast mechanism whose response decreases in strength with distance from the edge as, for example, in Mach or Hering inhibition (Fiorentini *et al.*, 1990). In summary, a possible, albeit cumbersome, account for the observed changes in the structure and magnitude of brightness induction as a function of test field height and width might include three mechanisms: (1) a GI mechanism (that is not a homogeneous fill-in mechanism) which accounts for patterned induction in the elongated test fields; (2) a homogeneous high-threshold fill-in mechanism which accounts for both the progressive flattening of the structure and the increasing magnitude of induction that begins at intermediate test field widths; and (3) an edge or border contrast mechanism that accounts for the "cusping" seen at the narrower test field widths.

A multiscale filtering explanation of GI and SBC

Perhaps a simpler and more plausible idea is that a mechanism dependent on the distribution of luminance over a broader area, not simply perimeter or border luminance, determines brightness induction. This hypothesis is consistent with the large number of studies which have indicated that regions removed from the test field edge play a significant role in both SBC (Heinemann, 1972; Arend *et al.*, 1971; Land & McCann, 1971; Shapley & Reid, 1985; Reid & Shapley, 1988) and GI (Foley & McCourt, 1985; Zaidi, 1989; Moulden & Kingdom, 1991; McCourt & Blakeslee, 1993). The convolution of a GI stimulus with a suitably chosen DOG weighting function will produce opposite-phase induced gratings. However, no single concentric weighting function produces counterphase induction across the combination of test field heights and inducing spatial frequencies for which it is observed (Foley & McCourt, 1985). Moulden & Kingdom (1991) suggested that a multiscale array of DOG filters could, however, explain many aspects of GI, including the discriminability of the inducing and induced stripes, and the rapid fall-off of induced grating amplitude with increasing inducing grating spatial frequency (McCourt, 1982) and test field height (McCourt, 1982; Foley & McCourt, 1985).

We revisit these ideas by posing the question: How accurately can the pooled output of DOG filters across multiple spatial scales account for the brightness matching data of the present experiment? To answer this question we selected an array of seven isotropic two-dimensional DOG filters whose center frequencies were arranged at octave intervals (see Table 1). The ratio of center–surround space constants was 1:2, producing filters whose spatial frequency bandwidth (full-width at half-height) was 1.9 octaves. Center–surround volumes were equal, such that the response of each DOG to a homogeneous field was zero. The particular filters employed were chosen by first setting the center size (zero-crossing to zero-crossing) of one of the filters of the array to 3 deg, thus matching the height of the intermediate test field (mechanism 5 of Table 1). Four additional filters (also arranged at octave intervals—two above and two below the 3 deg filter) were added to the array to ensure that the ensemble as a whole captured the majority of the Fourier energy contained in all of our stimuli at all test field heights (mechanisms 3, 4, 6 and 7). Finally, two high frequency filters (mechanisms 1 and 2) were added such that the array encompassed the high frequency range typically used in modeling the early filtering stages of the visual system (Wilson & Bergen, 1979; Watt & Morgan, 1985; Moulden & Kingdom, 1991; Kingdom & Moulden, 1992). The spatial parameters of our mechanisms, as well as those used in Moulden and Kingdom's (1991) model of grating induction, appear in Table 1. Note that the present filter

TABLE 1. Difference of gaussian space constants

	Space constant (deg)	
Mechanism	Center	Surround
1	0.047	0.093
2	0.094	0.188
3	0.188	0.375
4	0.375	0.75
5	0.75	1.5
6	1.5	3
7	3	6
Moulden & Kingdom (1991)		
1	0.033	0.052
2	0.065	0.104
3	0.130	0.208
4	0.262	0.419

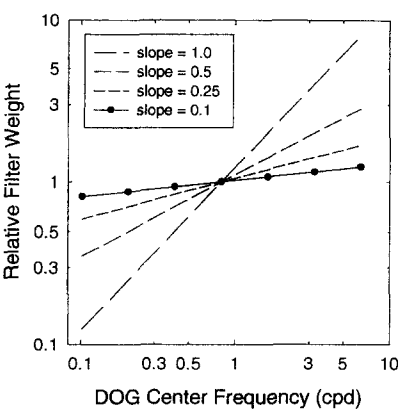

FIGURE 10. Potential weighting functions for combining filter outputs are illustrated by the power functions describing log filter weight as a function of log center frequency. A slope of 1.0 corresponds to the low-frequency fall-off of the human contrast sensitivity function at threshold (Campbell & Robson, 1969). Successively shallower slopes approximate the reduced low-frequency fall-off at suprathreshold contrast levels, as determined by contrast matching (Georgeson & Sullivan, 1975).

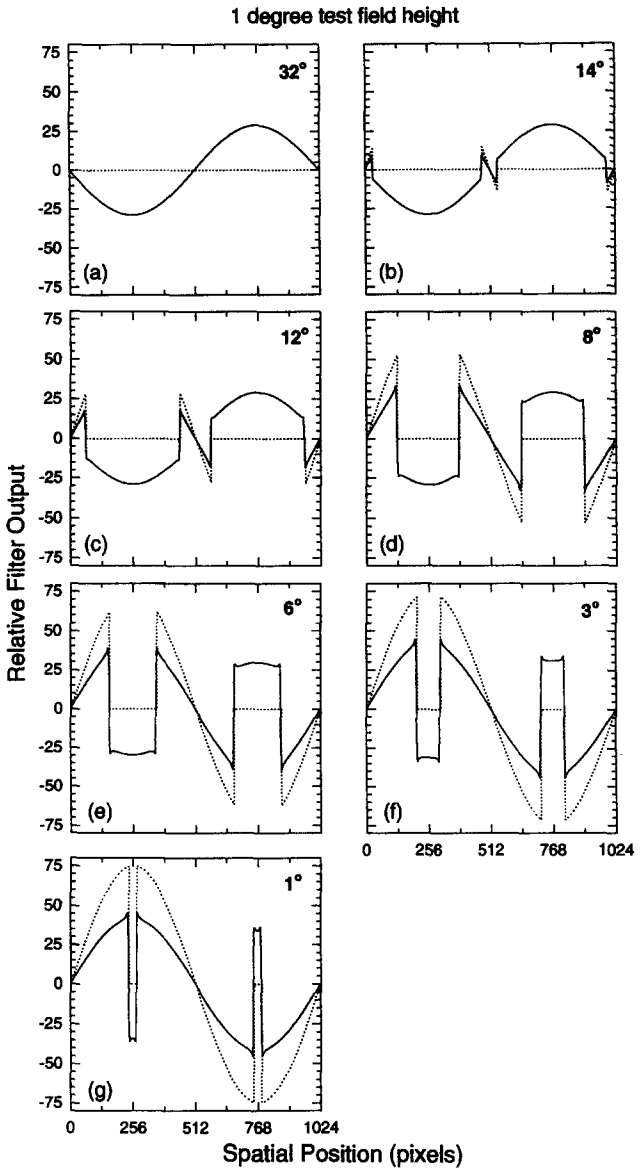

FIGURE 11. A slice through the summed convolution output of the weighted filter array (combined with a weighting slope of 0.1) for each of the test field widths in the 1 deg test field height condition. The dotted line depicts the veridical luminance profile of the stimulus display taken at the vertical center of the test field. The solid line is the summed convolution output along this same line.

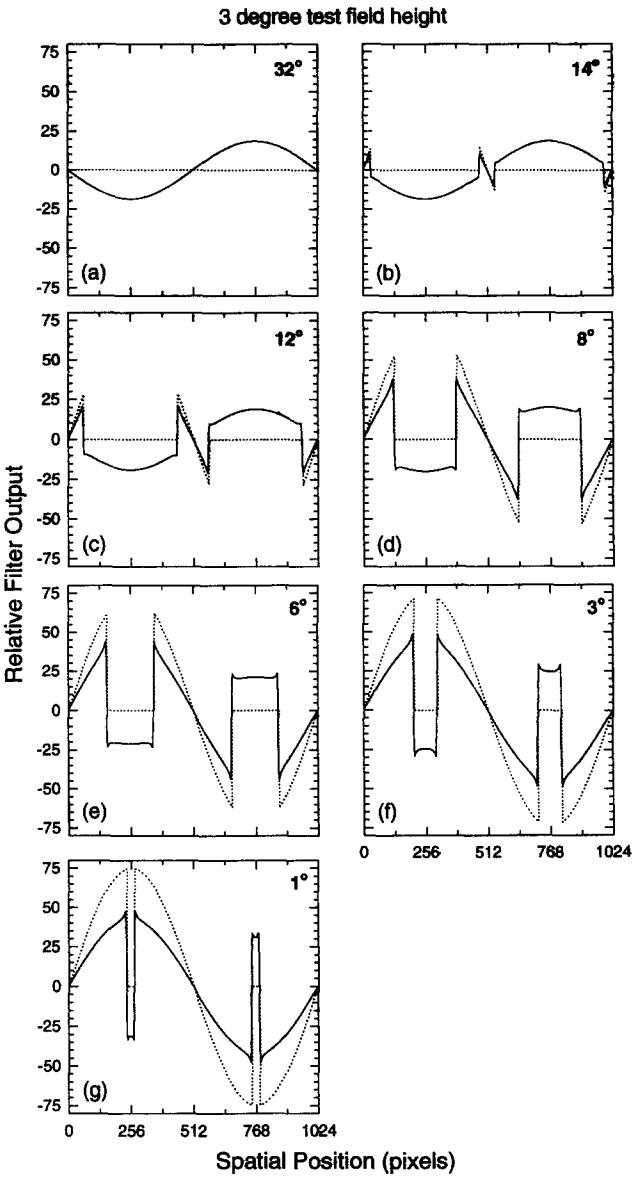

FIGURE 12. A slice through the summed convolution output of the weighted filter array (combined with a weighting slope = 0.1) for each of the test field widths in the 3 deg test field height condition. See Fig. 11 for details.

array extends to much lower spatial frequencies (by over an order of magnitude) than those used by Moulden & Kingdom (1991), who were modeling GI stimuli with both smaller test field heights (ranging between 0.2 and 1.6 deg), and higher spatial frequency inducing gratings (between 0.1 and 1.6 c/d). It should be noted that the particular filter center frequencies we have selected are not critical: any octave-interval (or denser) array of filters which spans a comparable range of frequency will produce essentially identical pooled responses.

How should the outputs of the different filters in the array be summed? A number of potential weighting functions are illustrated by the power functions depicted in Fig. 10, where log filter weight is plotted as a function of log center frequency. A weighting slope of 1.0 corresponds to the linear low-frequency fall-off of the human threshold contrast sensitivity function (Campbell & Robson, 1968; Laming, 1991). Successively shallower slopes approximate the reduced low-frequency fall-off in sensitivity observed at suprathreshold contrast levels, as determined by contrast matching (Georgeson & Sullivan, 1975). A comparison of the convolutions of filter arrays combined with weights ranging between 0 and 1.0 with the point-by-point brightness matching data of Figs 2–4 revealed that a weighting slope of 0.1 was optimal. This slope is quite consistent with the shallow low-frequency fall-off of the suprathreshold CSF, which is expected to be associated with our high suprathreshold contrast stimulus (0.75 contrast inducing grating, 0.00 contrast test field).

Figures 11–13 illustrate the summed output of the weighted filter array when convolved with the inducing stimuli. These profiles are taken along a line correspond-

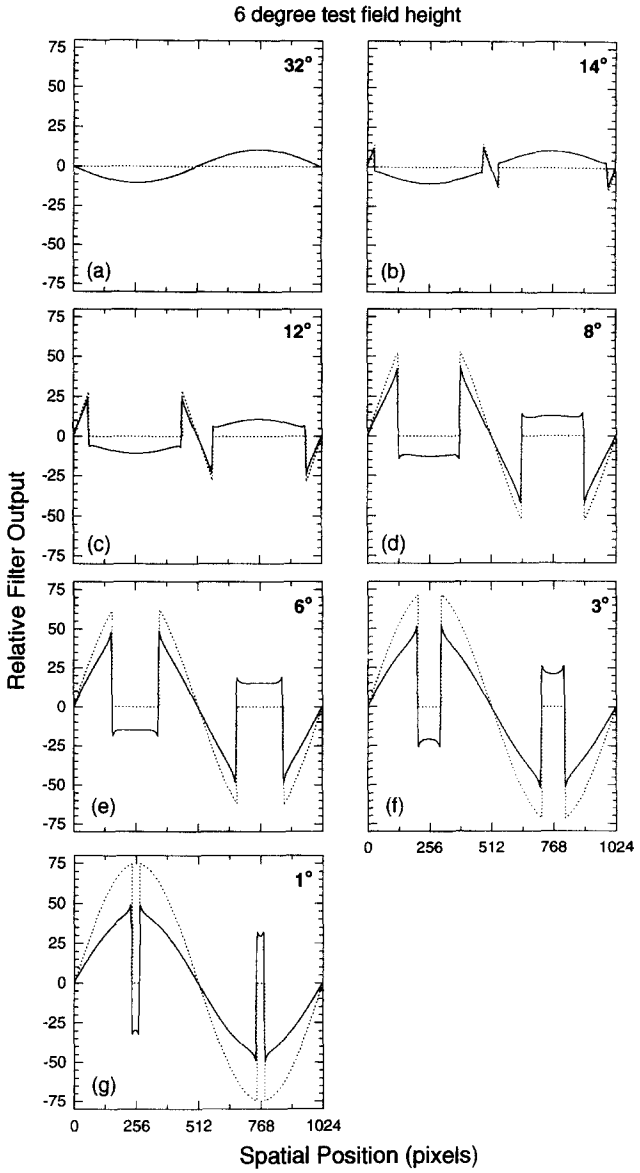

FIGURE 13. A slice through the summed convolution output of the weighted filter array (combined with a weighting slope = 0.1) for each of the test field widths in the 6 deg test field height condition. See Fig. 11 for details.

ing to the vertical center of the test field. A comparison of these convolutions with the matching data of Figs 2–4 clearly indicates that multiscale, weighted linear filtering captures all of the essential features of the matching data, in terms of both *structure* and *magnitude*. Notice that the predicted overall magnitude of induction decreases with increasing test field height, however, within each test field height the magnitude of induction increases with decreasing test field width. The filtering operation also captures the flattening and reverse cusping of the sinewave structure in the test fields that occurs with decreasing test field width, and the test field widths at which these structural changes occur. It is particularly noteworthy that the linear weighted combination of filter outputs simultaneously captures the undermatching to the inducing grating.

Applying the multiscale filtering explanation to other brightness phenomena

In order to test the generality of this simple filtering explanation we convolved this same filter set (using the identical weighting function) with the GI demonstrations of Zaidi (1989). Although intriguing, these observations have never been adequately explained. In one demonstration Zaidi (1989) showed that the orientation of induced gratings depended, not on the orientation of the inducing grating, but on the relative phase of the upper and lower inducing gratings. In the standard grating induction stimulus the upper and lower inducing gratings are in phase and the induced grating is a counterphase grating of the same orientation as the inducing grating [see Fig. 1(a)]. Zaidi (1989) found, however, that when the phase of the upper and lower gratings was slightly offset, the test field appeared to contain a *tilted* induced grating. The most pronounced orientation change occurred for upper and lower inducing gratings whose phase was offset by 90 deg [left panel of Fig. 14(a)]. When inducing gratings were offset by 180 deg the test field appeared to contain light and dark meniscuses, but no cohesive grating was perceived [left panel of Fig. 14(b)]. The right-hand panels of Fig. 14(a, b) are 3D mesh plots which show (in magnified view) the weighted test field output of the filter array following convolution with these stimuli. It is clear that the filter array produces an output which closely resembles the appearance of these two test fields.

In a second demonstration Zaidi (1989) showed that if the orientation and phase of four different spatial frequency inducing gratings were adjusted such that the horizontal spatial frequency at the test field edges was identical in all conditions, the gratings induced in the homogeneous test field were vertically oriented and possessed the same spatial frequency. Zaidi (1989) concluded that whereas the orientation and spatial frequency of the induced grating appeared to be governed by the proximal cues, GI magnitude depended on distal portions of the inducing grating as well, since the amplitude of induction increased markedly with increasing inducing grating elevation (i.e., as the orientation of the inducing grating became perpendicular to the test field). The left-hand panels of Fig. 15(a, b) illustrate examples of these stimuli for two inducing grating orientations (90 and 45 deg elevations, respectively). The right-hand panels again show 3D mesh plots which illustrate (in magnified view) the weighted test field output of the filter array following convolution with these stimuli. The output of this array of filters closely resembles the appearance of the test fields. Figure 16 plots the output of the weighted filter array (as relative test field contrast) as a function of inducing grating elevation. The systematic decrease in induction magnitude with decreasing inducing grating elevation produced by the linear array is strikingly similar to the data of Zaidi (1989).

To further test the generality of the weighted filter explanation we convolved the array with a stimulus similar to that used by Shapley & Reid (1985) and Reid &

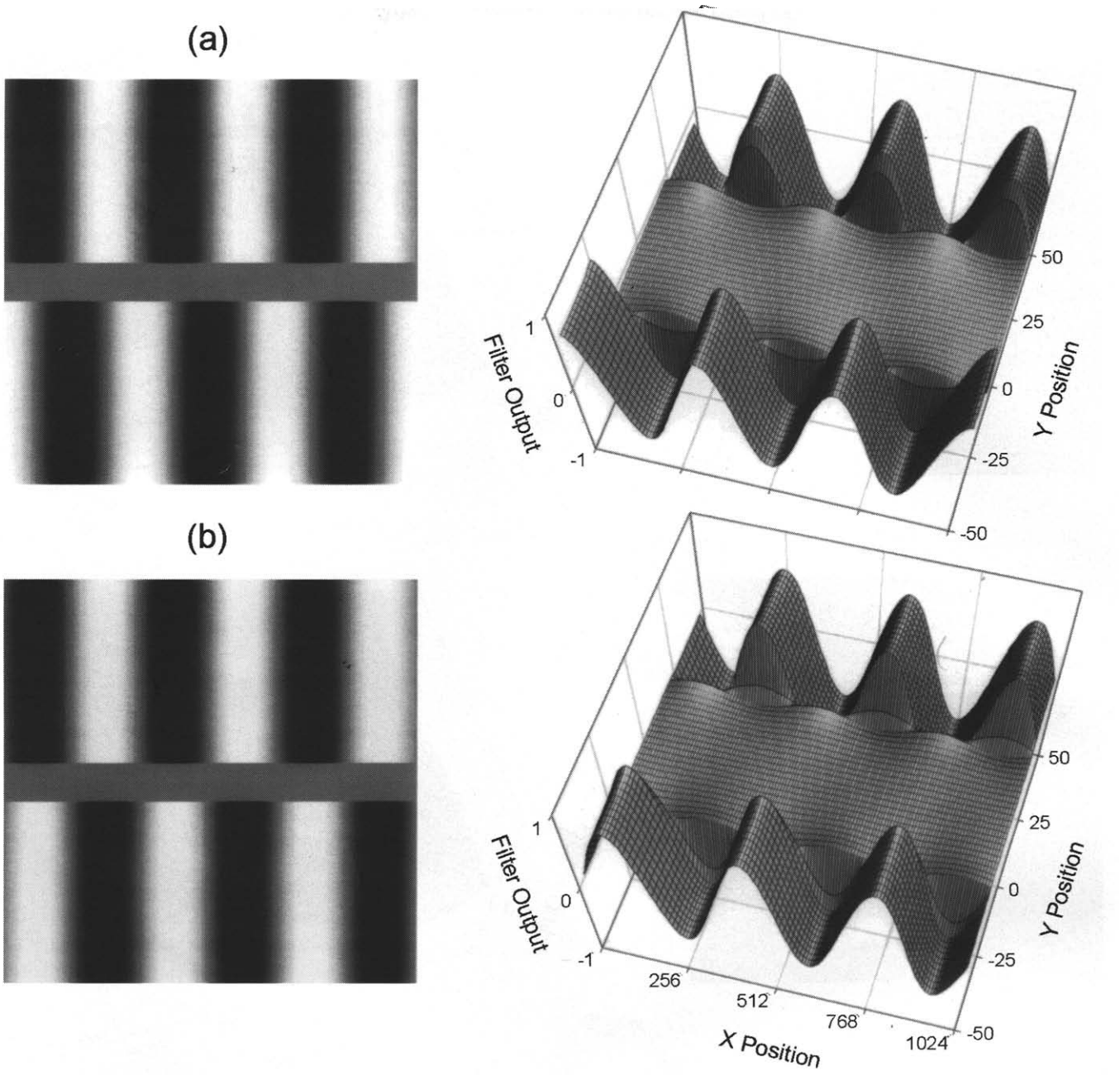

FIGURE 14. Zaidi's (1989) grating induction demonstration showing that (a, left panel) when the phase of the upper and lower inducing gratings is offset by 90 deg the test field appears to contain a tilted induced grating and (b, left panel) when the inducing gratings are offset by 180 deg the test field appears to consist of light and dark meniscuses, but no cohesive grating is perceived. The right-hand panels of (a) and (b) are 3D mesh plots which show (in magnified view) the weighted output of the filter array (weighting slope = 0.1) following convolution with the stimuli shown in the respective left-hand panels. It is clear that the filter array produces an output which closely resembles the appearance of the induced brightness in the two test fields.

Shapley (1988) to demonstrate the existence of brightness contrast and "assimilation". Assimilation is interpreted and modeled by these investigators as the summation of local contrasts across space. The left-hand panel of Fig. 17 presents a version of the stimulus used by Shapley & Reid (1985). The right-hand panel contains the luminance profile of this stimulus (dotted line), along the vertical center of the test fields. The solid line represents a slice of the weighted filter convolution output at the same location. The filter array produces output which accords with the appearance of both the equiluminant central test fields and the equiluminant surrounds.

Finally, the same weighted filter array also produces output which agrees with the appearance of the Hermann Grid stimulus across a variety of spatial scales. Figure 18 shows one of the stimulus configurations examined and a mesh plot of the weighted array output at one of the grid

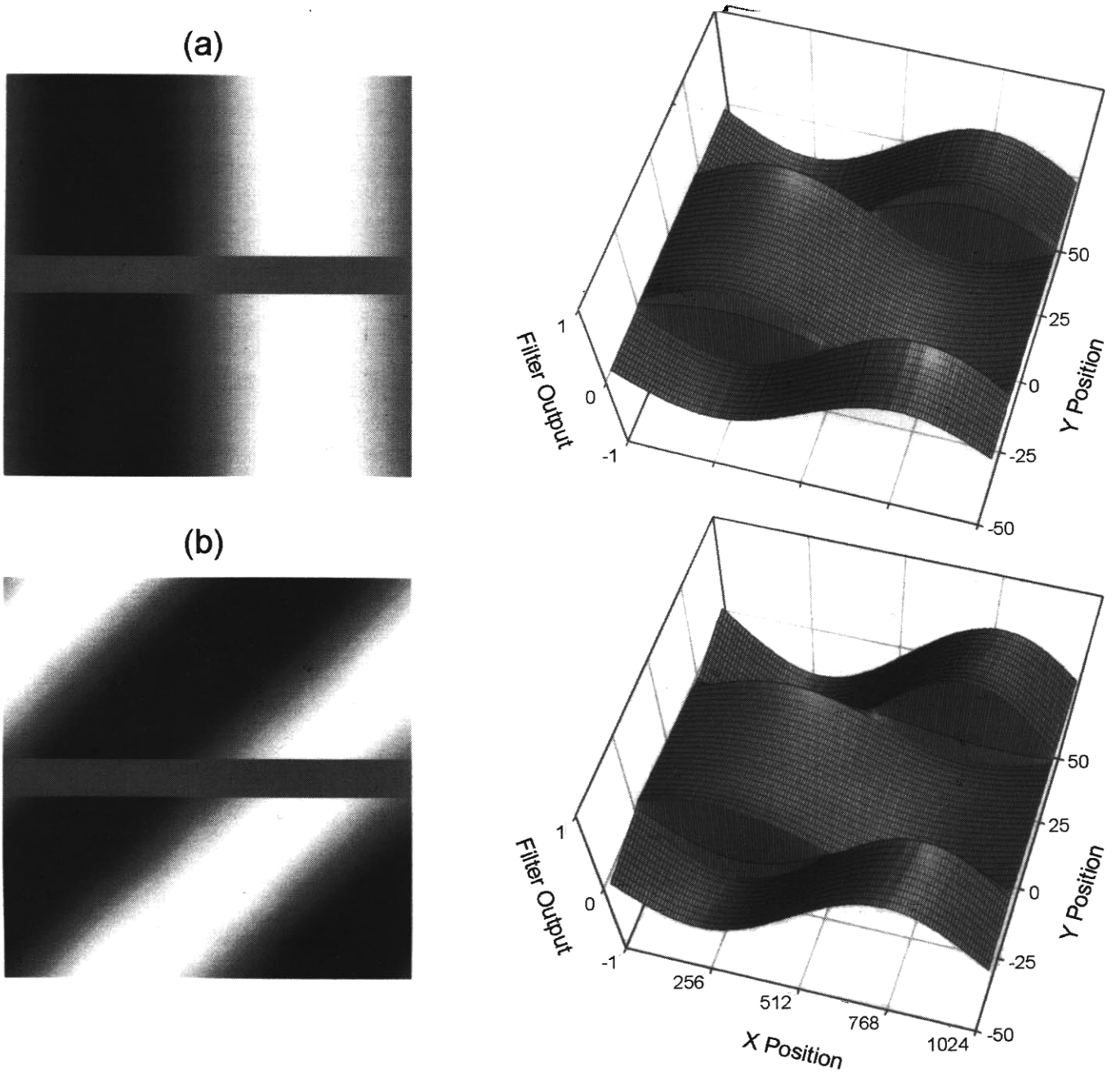

FIGURE 15. Two stimuli (left-hand panels a, b) like those used by Zaidi (1989) demonstrating that the orientation and spatial frequency of the induced grating appear to be governed by proximal cues. The spatial frequency of the gratings in (a) and (b) are different but their orientation and phase have been adjusted such that the horizontal spatial frequency at the test field edges is identical in both conditions. The gratings induced in the homogeneous test fields are vertically oriented and possess the same spatial frequency. The right-hand panels of (a) and (b) are 3D mesh plots of the weighted array output (weighting slope = 0.1) following convolution with the stimuli shown in the respective left-hand panels. The output of weighted filter array closely resembles the appearance of the induced brightness in the test fields.

intersections. The filter array produces localized output minima at the same locations where human observers see dark spots at the intersections of the "streets" of the grid.

In the interests of brevity (and because the linear filtering results appear to account so well for our observations) we have not attempted in this paper to refine the multiscale filter array explanation by attaching plausible response nonlinearities (such as a sigmoidal contrast transduction stage) to the filter outputs, or to explore nonlinear combination rules (such as Minkowski pooling) with regard to pooling filter outputs. Such extensions of the present explanation can, however, if merely by virtue of the greater number of degrees of freedom these added stages afford, only enhance the explanatory power of this general approach. We should note, however, that such response nonlinearities will be required to explain other salient intensive aspects of brightness induction, such as the saturation of induced

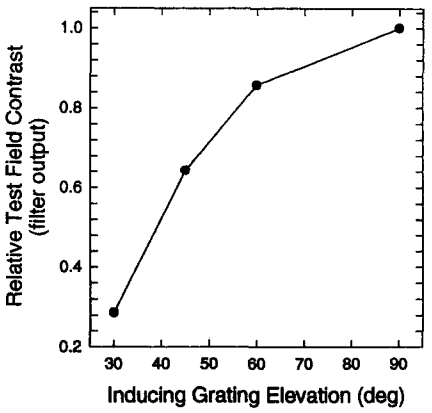

FIGURE 16. The output of the weighted filter array (weighting slope = 0.1) predicts the systematic decrease in induction magnitude which Zaidi (1989) reported occurred with decreasing inducing grating elevation. The stimuli were produced like those previously described and depicted in the left-hand panels of Fig. 15(a) 90 deg elevation and Fig. 15(b) 45 deg elevation, but included two additional stimuli with elevations of 30 and 60 deg.

contrast with increasing inducing grating contrast, the nonlinear relationship between matching contrast and test field contrast in GI displays (McCourt & Blakeslee, 1994), and the "crispening effect" (Whittle, 1992).

Utility of a multiscale filtering explanation

It would appear that a multiscale array of two-dimensional DOG filters whose outputs are weighted in accord with suprathreshold contrast sensitivity provides a powerful heuristic towards explaining a number of seemingly complex features of GI, while simultaneously encompassing salient features of induction in SBC, brightness assimilation and Hermann Grid stimuli. Since most brightness models (indeed, most models of spatial vision) incorporate spatial filtering at an early stage to extract information about luminance changes, it seems useful to categorize brightness phenomena according to which can or cannot be accounted for by multiscale filtering. For example, our multiscale filtering explanation cannot account for effects like the Craik–O'Brien–Cornsweet illusion or the appearance of the missing-fundamental squarewave at low contrasts. These types of brightness effects may indeed depend on a low-threshold border-dependent brightness fill-in mechanism such as that discussed by Burr (1987), or on more complex fill-in mechanisms or brightness assignment rules such as those incorporated in a number of other models (Grossberg & Todorovic, 1988; Kingdom & Moulden, 1992; Heinemann & Chase, 1995; Pessoa *et al.*, 1995).

Some brightness models exist which incorporate non-homogeneous fill-in mechanisms (Grossberg & Mingolla, 1987; Pessoa *et al.*, 1995). These models are based on the boundary contour system/feature contour system first proposed by Cohen & Grossberg (1984) and later elaborated by Grossberg and Mingolla (Grossberg & Mingolla, 1985, 1987). In these models, as in homogeneous fill-in models, boundary signals are used to generate fill-in compartments within which brightness is diffused or spread such that, at equilibrium, the diffused activities correspond to perceived brightness. The most recent versions of these models, however, have been modified such that the boundary signals may be generated either by luminance "edges" or by continuous luminance gradients. In the latter case, luminance

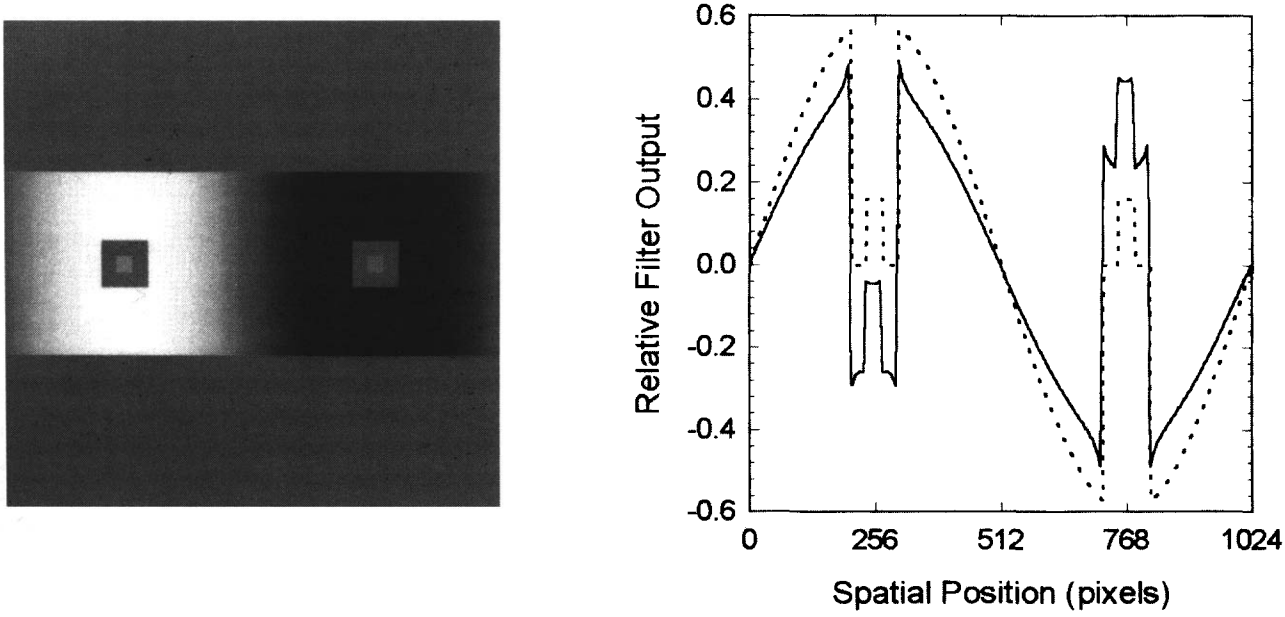

FIGURE 17. A version of the stimulus used by Shapley & Reid (1985) to demonstrate brightness contrast and "assimilation" (left-hand panel). In the right-hand panel the luminance profile of this stimulus taken at the vertical center of the test fields is depicted by the dotted line. The solid line represents a slice (taken at the same location) of the output of the weighted filter array (weighting slope = 0.1) following convolution with this stimulus. It is clear that the output of the weighted filter array predicts the appearance of both the equiluminant central test fields and the equiluminant surrounds.

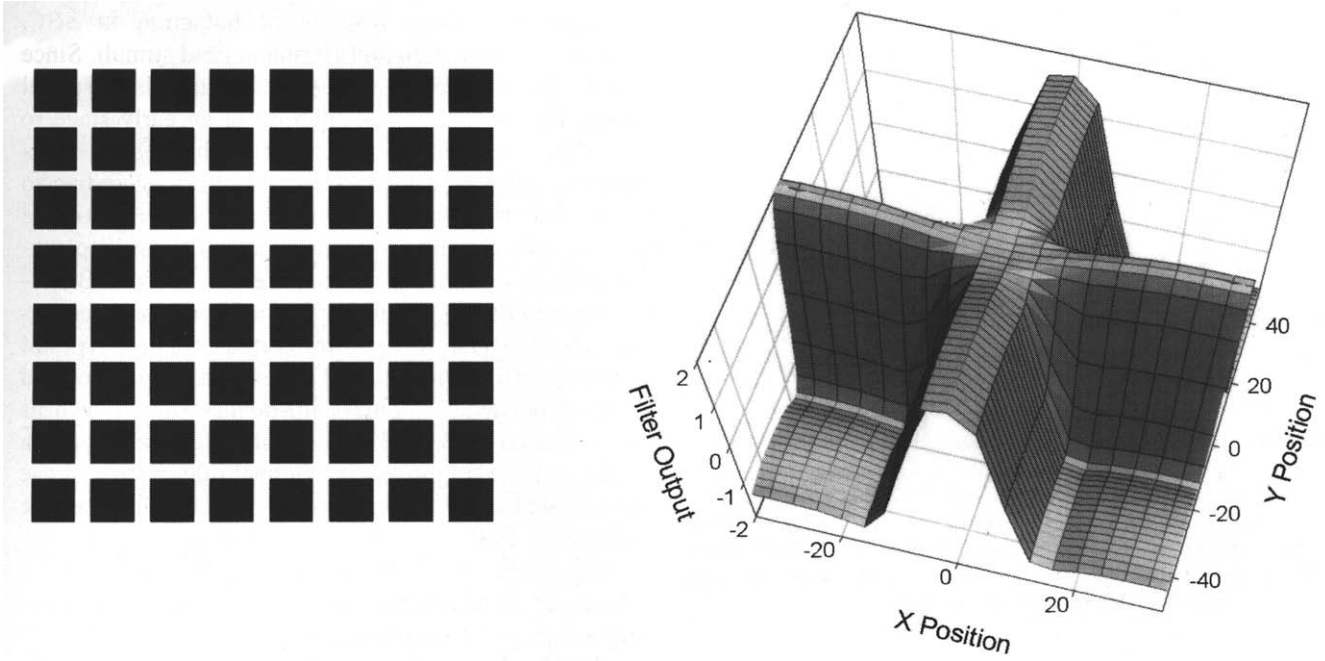

FIGURE 18. This example of the Hermann Grid stimulus (left-hand panel) was convolved with the weighted filter array (weighting slope = 0.1). The right-hand panel shows a mesh plot of the weighted filter array output at one of the intersections. The filter array produces localized output minima at the same locations where human observers see dark spots at the intersections of the "streets" of the grid.

gradients produce "boundary webs" which may partially or totally arrest diffusion within specified regions, thus allowing fill-in to account for gradual changes in brightness across space (Grossberg & Mingolla, 1987; Pessoa *et al.*, 1995). Interestingly, while in regions of zero boundary activity brightness is free to diffuse (as in the original homogeneous fill-in models), diffusion is inhibited in regions where boundary web signals are dense, and the predicted brightness distribution reverts to that produced by the outputs of the initial filtering operations (Pessoa *et al.*, 1995). While it is possible that these more complex models may also account for brightness induction in the present study, it is clear that understanding these effects does not *require* an explanation beyond multiscale spatial filtering.

Physiological plausibility

Although center–surround filtering is one of the oldest and most frequently invoked mechanisms used to explain induction effects (Kingdom *et al.*, 1997; for review see Fiorentini *et al.*, 1990) it is often dismissed as an explanation for long-range effects such as SBC [and Shapley and Reid's (1985) demonstration of assimilation] because physiological evidence has indicated that retinal and/or LGN receptive fields are too small to account for the distances over which these brightness effects occur (Shapley & Enroth-Cugell, 1984; Cornsweet & Teller, 1965; Reid & Shapley, 1988; Grossberg & Todorovic, 1988; Rossi & Paradiso, 1996; Paradiso & Hahn, 1996; for reviews see Kingdom & Moulden, 1988; Fiorentini *et al.*, 1990). While the receptive fields corresponding to the largest DOG filters used in this study do not appear to exist at the level of the retina, it may be premature to altogether reject the notion that such filters might exist at those levels of the nervous system where brightness percepts are determined. Recent evidence in fact suggests that a significant number of cells in cat primary visual cortex respond in a manner correlated with perceived brightness, and that they do so over distances far exceeding the size of their "classical" receptive fields mapped using conventional techniques (Rossi *et al.*, 1996). This was demonstrated using a dynamic version of brightness induction in which a central gray test patch was flanked by a surround whose luminance was temporally modulated. In human observers this stimulus gives rise to a strong brightness modulation of the test patch (DeValois *et al.*, 1986). Even under conditions in which the central test patch extended 3 deg or more to either side of the "classical" receptive field borders, inclusive of any end-stopping regions, such that the receptive field of the cortical cell fell entirely within the homogeneous test field, the cell's output correlated with test patch brightness (as opposed to luminance). Interestingly, these are precisely the conditions under which it has long been assumed that a cell would not respond to a SBC stimulus and which necessitated the proposal of explanatory mechanisms such as border-dependent brightness fill-in over large regions. The results of Rossi *et al.* (1996) suggest that brightness may be synthesized at an early stage in the striate cortex, and that extensive "silent surrounds" may contribute to brightness processing. Importantly, the authors note that these neurons should not be regarded as "brightness detectors" *per se*, but rather as multiplexing brightness information along with other stimulus attributes such as orientation and spatial frequency. Recent

evidence from primate anatomy and physiology also indicates that at the earliest cortical levels (V1) the substrate exists for providing cells with input from relatively large regions of the visual field, and that the response properties of cells are modulated by stimuli lying far outside the "classical" receptive field (Gilbert *et al.*, 1996). Thus, it appears that heretofore unappreciated lateral interactions in early visual processing may provide an order-of-magnitude-larger area of visual integration than that revealed by the "classical" receptive field, making the inclusion of large filters in a multiscale array less implausible than previously believed.

REFERENCES

Arend, L. E., Buehler, J. N. & Lockhead, G. R. (1971). Difference information in brightness perception. *Perception and Psychophysics, 9*, 367–370.

Arend, L. E. & Spehar, B. (1993a) Lightness, brightness, and brightness contrast: 1. Illuminance variation. *Perception and Psychophysics, 54*, 446–456.

Arend, L. E. & Spehar, B. (1993b) Lightness, brightness, and brightness contrast: 2. Reflectance variation. *Perception and Psychophysics, 54*, 457–468.

Burr, D. (1987). Implications of the Craik–O'Brien illusion for brightness perception. *Vision Research, 27*, 1903–1913.

Campbell, F. W. & Robson, J. G. (1968). Application of Fourier analysis to the visibility of gratings. *Journal of Physiology (London), 197*, 551–566.

Cohen, M. & Grossberg, S. (1984). Neural dynamics of brightness perception: features, boundaries, diffusion, and resonance. *Perception and Psychophysics, 36*, 428–456.

Cornsweet, T. N. & Teller, D. (1965). Relation of increment thresholds to brightness and luminance. *Journal of the Optical Society of America, 55*, 1303–1308.

DeValois, R. L. & DeValois, K. K. (1988). *Spatial vision*. New York: Oxford University Press.

DeValois, R. L. & Pease, P. L. (1971). Contours and contrast: responses of monkey lateral geniculate cells to luminance and color figures. *Science, 171*, 694–696.

DeValois, R. L., Webster, M. A., DeValois, K. K. & Lingelbach, B. (1986). Temporal properties of brightness and color induction. *Vision Research, 26*, 887–897.

Fiorentini, A., Baumgartner, G., Magnussen, S., Schiller, P. H. & Thomas, J. P. (1990). The perception of brightness and darkness: relations to neuronal receptive fields. In Spillmann, L. & Werner J. S. (Eds), *Visual perception: the neurophysiological foundations*. San Diego: Academic Press.

Foley, J. M. & McCourt, M. E. (1985). Visual grating induction. *Journal of the Optical Society of America A, 2*, 1220–1230.

Georgeson, M. A. & Sullivan, G. D. (1975). Contrast constancy: deblurring in human vision by spatial frequency channels. *Journal of Physiology (London), 252*, 627–656.

Gilbert, C. D., Anirudda, D., Minami, I., Kapadia, M. & Westheimer, G. (1996). Spatial integration and cortical dynamics. *Proceedings of the National Academy of Sciences USA, 93*, 615–622.

Grossberg, S. & Mingolla, E. (1985). Neural dynamics of form perception: boundary completion, illusory figures, and neon color spreading. *Psychological Review, 92*, 173–211.

Grossberg, S. & Mingolla, E. (1987). Neural dynamics of surface perception: boundary webs, illuminants, and shape-from-shading. *Computer Vision, Graphics, and Image Processing, 37*, 116–165.

Grossberg, S. & Todorovic, D. (1988). Neural dynamics of 1-D and 2-D brightness perception: a unified model of classical and recent phenomena. *Perception and Psychophysics, 43*, 241–277.

Heinemann, E. G. (1955). Simultaneous brightness induction as a function of inducing and test-field luminances. *Journal of Experimental Psychology, 50*, 89–96.

Heinemann, E. G. (1972). Simultaneous brightness induction. In Jameson, D. & Hurvich L. M. (Eds), *Handbook of sensory physiology, VII-4. Visual psychophysics*. Berlin: Springer.

Heinemann, E. G. & Chase, S. (1995). A quantitative model for simultaneous brightness induction. *Vision Research, 35*, 2007–2020.

Kingdom, F. A. A., McCourt, M. E. & Blakeslee, B. (1997). In defense of lateral inhibition as the underlying cause of induced brightness effects: A reply to Spehar, Gilchrist & Arend. *Vision Research, 37*, 1039–1044.

Kingdom, F. A.A. & Moulden, B. (1988). Border effects on brightness: a review of findings, models and issues. *Spatial Vision, 3*, 225–262.

Kingdom, F. A.A. & Moulden, B. (1992). A multi-channel approach to brightness coding. *Vision Research, 32*, 1565–1582.

Laming, D. (1991). Spatial frequency channels. In Kulikowski, J. J., Walsh, V. & Murray, I. J. (Eds), *Vision and visual dysfunction Vol 5. Limits of vision* (pp. 97–105). Boca Raton, FL: CRC Press.

Land, E. H. & McCann, J. J. (1971). The retinex theory of vision. *Journal of the Optical Society of America, 61*, 1–11.

McCourt, M. E. (1982). A spatial frequency dependent grating-induction effect. *Vision Research, 22*, 119–134.

McCourt, M. E. (1994). Grating induction: a new explanation for stationary visual phantoms. *Vision Research, 34*, 1609–1618.

McCourt, M. E. & Blakeslee, B. (1993). The effect of edge blur on grating induction magnitude. *Vision Research, 33*, 2499–2507.

McCourt, M.E. & Blakeslee, B. (1994). A contrast matching analysis of grating induction and suprathreshold contrast perception. *Journal of the Optical Society of America A, 11*, 14–24.

Moulden, B. & Kingdom, F. A.A. (1991). The local border mechanism in grating induction. *Vision Research, 31*, 1999–2008.

Paradiso, M. A. & Hahn, S. (1996). Filling-in percepts produced by luminance modulation. *Vision Research, 36*, 2657–2663.

Paradiso, M. A. & Nakayama, K. (1991). Brightness perception and filling-in. *Vision Research, 31*, 1221–1236.

Pessoa, L., Mingolla, E. & Neumann, H. (1995). A contrast- and luminance-driven multiscale network model of brightness perception. *Vision Research, 35*, 2201–2223.

Reid, C. R. & Shapley, R. (1988). Brightness induction by local contrast and the spatial dependence of assimilation. *Vision Research, 28*, 115–132.

Rossi, A. F. & Paradiso, M. A. (1996). Temporal limits of brightness induction and mechanisms of brightness perception. *Vision Research, 36*, 1391–1398.

Rossi, A. F., Rittenhouse, C. D. & Paradiso, M. A. (1996). The representation of brightness in primary visual cortex. *Science, 273*, 1104–1107.

Shapley, R. & Enroth-Cugell, C. (1984). Visual adaptation and retinal gain-controls. *Progress in Retinal Research, 3*, 263–346.

Shapley, R. & Reid, R.C. (1985). Contrast and assimilation in the perception of brightness. *Proceedings of the National Academy of Sciences USA, 82*, 5983–5986.

Watt, R. J. & Morgan, M. J. (1985). A theory of the primitive spatial code in human vision. *Vision Research, 25*, 1661–1674.

Whittle, P. (1992). Brightness, discriminability and the "crispening effect". *Vision Research, 32*, 1493–1507.

Wilson, H. R. & Bergen, J. R. (1979). A four-mechanism model for threshold spatial vision. *Vision Research, 19*, 19–32.

Yund, E. W. & Armington, J. C. (1975). Color and brightness contrast effects as a function of spatial variables. *Vision Research, 15*, 917–929.

Yund, E. W., Snodderly, D. M., Hepler, N. K. & DeValois, R. L. (1977). Brightness contrast effects in monkey lateral geniculate nucleus. *Sensory Processes, 1*, 260–271.

Zaidi, Q. (1989). Local and distal factors in visual grating induction. *Vision Research, 29*, 691–697.

Acknowledgements—Supported by grants from NSF to B. Blakeslee (IBN-9306776 and IBN-9514201) and by grants from NIH (EY-1013301) to M. McCourt and B. Blakeslee and AFOSR (F49620-94-1-0445).